TYPE 2 DEIODINASE POLYMORPHISM CAUSES ER STRESS AND HYPOTHYROIDISM IN THE BRAIN

Sungro Jo[1,2], Tatiana L. Fonseca[1,3], Barbara M. L. C. Bocco[1,3], Gustavo W. Fernandes[3], Elizabeth A. McAninch[2], Anaysa P. Bolin[2,4], Rodrigo R. Da Conceição[2,5], Joao Pedro W. S. De Castro[2], Daniele L. Ignacio[2], Péter Egri[6], Dorottya Németh[6], Csaba Fekete[6], Maria Martha Bernardi[7], Victoria D. Leitch[8], Naila S. Mannan[8], Katharine F. Curry[8], Natalie C. Butterfield[8], J. H. Duncan Bassett[8], Graham R. Williams[8], Balázs Gereben[6], Miriam O. Ribeiro[9], Antonio C. Bianco[3]

[2]Division of Endocrinology and Metabolism, Rush University Medical Center, Chicago, IL;
[3]Section of Adult & Pediatric Endocrinology, Diabetes & Metabolism, Department of Medicine, University of Chicago, Chicago IL
[4]Department of Pharmacology, Biomedical Science Institute, University of São Paulo, São Paulo, SP, Brazil;
[5]Laboratory of Molecular and Translational Endocrinology, Department of Medicine, Federal University of São Paulo, São Paulo, SP, Brazil;
[6]Department of Endocrine Neurobiology, Institute of Experimental Medicine, Hungarian Academy of Sciences, Budapest, Hungary;
[7]Graduate Program of Environmental and Experimental Pathology, Graduate Program of Dentistry, Universidade Paulista, Sao Paulo, SP, Brazil;
[8]Molecular Endocrinology Laboratory, Department of Medicine, Imperial College London, London, UK
[9]Developmental Disorders Program, Center of Biological Science and Health, Mackenzie Presbyterian University, Sao Paulo, SP, Brazil

[1]authors contributed equally to this work

Corresponding author:
Antonio C. Bianco, MD, PhD
Section of Adult & Pediatric Endocrinology, Diabetes & Metabolism,
University of Chicago Medical Center
5841 S. Maryland Ave.
MC1027, Room M267 | Chicago, IL 60637
Phone: 773-702-7234
email: abianco@deiodinase.org

Conflict of interest statement: Dr. Bianco is a consultant for Sentier LLC and Synthonics Inc; the other authors have declared that no conflict of interest exist.

Levothyroxine (LT4) is a form of thyroid hormone used to treat hypothyroidism. In the brain, T4 is converted to the active form T3 by the type 2 deiodinase (D2). Thus, it is intriguing that carriers of the Thr92Ala polymorphism in the D2 gene (*DIO2*) exhibit clinical improvement when liothyronine (LT3) is added to LT4 therapy. Here we report that D2 is a cargo protein in endoplasmic reticulum Golgi intermediary compartment (ERGIC) vesicles, recycling between ER and Golgi. The Thr92 to Ala substitution (Ala92-D2) caused ER stress and activated the unfolded protein response (UPR); Ala92-D2 accumulated in the trans-Golgi and generated less T3, all of which was restored by eliminating ER stress with the chemical chaperone 4-phenyl butyric acid (4-PBA). An Ala92-Dio2 polymorphism-carrying mouse exhibited UPR and hypothyroidism in distinct brain areas. The mouse refrained from physical activity, slept more and required additional time to memorize objects. Enhancing T3 signaling in the brain with LT3 improved cognition, whereas restoring proteostasis with 4-PBA eliminated the Ala92-Dio2 phenotype. In contrast, primary hypothyroidism intensified the Ala92-Dio2 phenotype, with only partial response to LT4 therapy. Disruption of cellular proteostasis and reduced Ala92-D2 activity may explain the failure of LT4 therapy in carriers of Thr92Ala-DIO2.

Introduction

Hypothyroidism results from autoimmune destruction or surgical removal of the thyroid gland. Hence, symptoms are due to insufficient levels of thyroid hormones and affect tens of millions worldwide (1). T4 is the main hormone secreted by the normal thyroid gland but it needs to be converted to T3 in order to gain full biological activity (2, 3). In healthy individuals the thyroid gland contributes only a small fraction of the daily T3 production (<20%); the bulk of T3 production happens outside the thyroid parenchyma via conversion from T4 by two deiodinases, D1 and D2. Thus, daily tablets of levothyroxine (LT4) to treat hypothyroidism is commonsensical, having evolved to be the standard of care for this disease (1, 4).

About 15% of LT4 treated hypothyroid patients remain symptomatic with impaired cognition and reduced physical activity despite appropriate treatment (5). The origin of these symptoms is not clear, with some speculating that LT4 therapy is not sufficient for all patients; thus symptoms may be due to residual hypothyroidism. In fact, LT4-treated hypothyroid patients lack thyroidal T3 secretion; all T3 is produced in tissues other than the thyroid gland, mostly via D2. While it has been assumed that deiodinases restore T3 homeostasis in LT4-treated patients (6), preclinical and clinical studies indicate that this pathway alone is not sufficient to fully restore daily T3 production during LT4 therapy (7-10).

Thyroidectomized rats on LT4 exhibit hypothyroidism in the liver, skeletal muscle and brain, despite normal serum TSH levels (8). Individuals on LT4 with normal serum TSH exhibit higher BMI, greater use of beta-blockers, statins or antidepressant medication (9) and lower energy expenditure (11); they also exhibit difficulty in weight management, fatigue or low energy levels, and problems with mood and memory (12). The brain, in particular, depends on T3 produced via the D2 pathway, which is located in glial cells. Indeed, most T3 bound to nuclear thyroid hormone receptors (TR) in the brain is produced locally via the D2 pathway (13). This occurs via a paracrine signaling mechanism in which glial cell-derived T3 activates neuronal gene expression (14). Thus, adequate D2 functionality is critical in LT4 treatment for hypothyroid patients, producing most circulating T3 and also directly impacting intracellular T3 levels.

D2 is a type-I endoplasmic reticulum (ER)-resident protein, what enables D2-generated T3 to access and bind TRs (3). D2 is atypical among the deiodinases in that it displays a relatively short half-life as a result of ubiquitination and proteasomal degradation. This is caused by an exclusive 18-residue loop that mediates binding to two ubiquitin ligases (15-17). This loop also harbors a Thr92 to Ala substitution caused by a SNP present in 12-36 % of the population (18). Not surprisingly, the single amino acid substitution slows down the rate of D2 turnover; it is also associated with ectopic presence of D2 in the Golgi apparatus (19). Clinically, carriers of the Thr92Ala-DIO2 polymorphism were found more likely to have hypertension, insulin resistance, type 2 diabetes, bipolar disorder, mental retardation, low IQ, recovery from lung injury, osteoarthritis, Alzheimer's disease (20) and increased bone turnover, but perhaps unsurprisingly, these associations have not been reproduced in all population studies (6, 21). It is intriguing however that carriers of the Thr92Ala polymorphism in *DIO2* (D2 gene) exhibited symptomatic

improvement when liothyronine (LT3) was added to LT4 therapy (22, 23), suggesting that Thr92Ala-DIO2 carriers do not produce sufficient amounts of T3 via D2. Indeed, two studies suggest that Thr92Ala-D2 is less catalytically active (24, 25), potentially explaining why only a small percentage of the LT4-treated hypothyroid patients exhibit residual symptoms.

Here we studied the Thr92Ala polymorphism in cell and animal models, having found that D2 is a cargo protein in ER Golgi intermediary compartment (ERGIC) vesicles, recycling between ER and Golgi. The Thr92 to Ala substitution (Ala92-D2) causes ER stress and activates the unfolded protein response (UPR) in different brain areas. Our findings suggest that disruption of cellular proteostasis and reduced Ala92-D2 catalytic activity explain the failure of LT4 therapy in carriers of the Thr92Ala-DIO2 polymorphism; the data support further studies with chemical chaperones and combination therapy with LT3 in humans.

Results

To understand how the Thr92Ala-DIO2 affects D2, we studied HEK-293 cells stably expressing either form of D2 double tagged with His and YFP (19). Thr92-D2^{HY} distributes predominantly to the ER with low level co-localization with the cis-Golgi marker GM130 (Figure 1A-C) and the trans-Golgi marker p230 (Figure 1D-F). Whereas Ala92-D2^{HY} also exhibits low level co-localization with the cis-Golgi marker (Figure 1G-I), it is clearly present in the trans-Golgi (Figure 1J-L).

A network of ERGIC vesicles exists that shuttles proteins back and forth between ER and cis-Golgi, namely the COP-II and COP-I vesicles (26, 27). COPII-vesicles recognize, concentrate and export ER proteins to the Golgi (28) based on the presence of export-signals, none of which can be found in D2. Other proteins are concentrated in COPII-vesicles via specific transport adaptors (29). To find out if D2 traffics through this network, we analyzed pull downs of both Thr92-D2^{HY} and Ala92-D2^{HY}. While we failed to identify COPII-proteins (data not shown), these pull downs contained the transport adaptor ERGIC53 (30) along with p97 and UBXD-1. p97 is an ATP-driven chaperone involved in quality control that uses adaptors to process ubiquitinated proteins for recycling or degradation (31). For example, p97 and the adaptor Atx-3 bind to and direct D2 to the proteasomes (32). Here, we saw that both Thr92-D2^{HY} and Ala92-D2^{HY} pull downs contain the p97 adaptor UBXD-1, known to bind ERGIC53 (33) (Figure. 1M-N). Thus, both forms of D2 can be directed to the ERGIC via interaction with the p97-UBXD-1-ERGIC-53 complex. The 18-residue loop in D2 (15) is also critical for interaction with p97-UBXD-1: its truncation (Δ18-D2^{HY}) prevents ERGIC53 pull down (Figure 1O) and reduces by ~30% colocalization with GM130 (Figure 1P-S).

Scanning the D2 sequence led us to two carboxyl target dibasic peptide ER-retrieval motifs, i.e. S<u>KR</u>U<u>KK</u>TR (34, 35). Indeed, truncation of this sequence (Δ10C-ThrD2^{HY} or Δ10C-AlaD2^{HY}) increases colocalization with GM130 by ~50% (Figure 1S-Z). Altogether, these studies indicate that a bidirectional traffic of D2 between ER and Golgi exists, with both Thr92-D2^{HY} and Ala92-

$D2^{HY}$ recycling between ER and Golgi. These observations, however, do not explain why or how only Ala92-$D2^{HY}$ accumulates in the trans-Golgi network.

ER stress pushes Ala92-$D2^{HY}$ to the trans-Golgi

Ala92-$D2^{HY}$ exhibits a longer half-life (19), an indication that the Thr92 to Ala substitution slows D2 targeting to the proteasome and could lead to its detrimental accumulation in the ER. Indeed, we detected UPR in Ala92-$D2^{HY}$-cells (Figure 2A-N). In these cells there is mostly activation of the IRE1α and ATF6 pathways that increase protein folding ability via chaperones and degradation of misfolded proteins. There is a ~2-fold increase in IRE1α phosphorylation (Figure 2A-B) and a ~3-fold increase in spliced *XBP1* (*sXBP1)* mRNA levels (Figure 2C) in cells expressing Ala92-$D2^{HY}$. While levels of un-cleaved ATF6 protein remain stable (Figure 2D), there is a ~2-fold increase in cleaved ATF6 protein (Figure 2D-E) and the mRNA levels of its downstream targets *CHOP* (~3-fold; Figure 2F) as well as the ER chaperone/folding protein BIP (~4-fold; Figure 2G-I). PERK phosphorylation (Figure 2J-K), which attenuates protein synthesis, as well as its downstream targets such as EIF2α phosphorylation (Figure 2L-M) and *ATF4* mRNA levels are not affected (Figure 2N).

In some settings, the Golgi quality control contributes with UPR by capturing misfolded proteins that emanate from the ER, diverting them for lysosomal degradation (36). In fact, it is known that cleaved ATF6 induces ERGIC53 expression (37) and its redistribution closer to the cis-Golgi (38), both features present in cells expressing Ala92-$D2^{HY}$. Here we found a 2.2-fold increase in ERGIC53 protein levels (Figure 2O-P) and a 50% increase in *ERGIC53* mRNA levels (Figure 2Q). The images confirm an increase in ERGIC53 protein (Figure 2R-S) revealing a ~35% higher colocalization with GM130 (Figure 2T-X) and indicating redistribution to cis-Golgi. Furthermore, colocalization between Ala92-$D2^{HY}$ and GM130 is ~30% lower in *ERGIC53*$^{-/-}$ cells (Figure 3A-H), confirming that ERGIC53 is involved in the distribution of Ala92-$D2^{HY}$ to the Golgi.

The 18-residue loop in D2 mediates binding to the WD-40 domain in WSB1, a D2 ubiquitin ligase (15, 16, 39). Typically, WD40 domains exhibit low level of sequence conservation, making them promiscuous binding partners (40). Therefore, we tested whether Ala92-$D2^{HY}$ interacts with other ER WD40-containing proteins that could provide an additional exit-route to the Golgi. The SREBP cleavage-activating protein (SCAP) is a WD40-containing ER cholesterol sensor that transports SREBP1 via ERGIC (41) to the Golgi (42), a pathway that is activated by ER stress(43, 44). Fluorescence resonance energy transfer (FRET) studies in live cells indicate that Ala92-$D2^{HY}$, but not Thr92-$D2^{HY}$, interacts with $SCAP^{ECFP}$ (ECFP in the carboxyl end) in cells depleted of cholesterol (Figure 3I) through a mechanism that requires the WD40 domain in SCAP (Figure 3J).

To find out how much the presence of Ala92-$D2^{HY}$ in the trans-Golgi depends on ER stress and/or SCAP activation, we explored whether overnight incubation of Ala92-$D2^{HY}$ cells with (i) the chemical chaperone 4-PBA or (ii) cholesterol excess, affected colocalization of Ala92-$D2^{HY}$ and p230. Indeed, exposure to 4-PBA normalized UPR markers (Table S1) and brought colocalization of Ala92-$D2^{HY}$ and p230 to the level observed in Thr92-$D2^{HY}$ cells (Figure 3K-Q). At the

same time, saturation with cholesterol reduced p230/Ala92-D2^{HY} colocalization by ~20% (Figure 3R-X). These data strengthen the argument that distribution of Ala92-D2^{HY} to the trans-Golgi is caused by ER stress and could involve the SCAP pathway.

Brain UPR in a mouse carrier of the Thr92Ala-Dio2 polymorphism

Five of the 6 critical amino acids in D2's 18-residue loop are conserved (17) in humans (92-TEGGDN-97) and mice (92-PESGNN-97): 93-E, 95-G, 97-N are the same, and 96-D/N is a conserved substitution. Because P occupies position 92 in murine D2, Thr92-Dio2 and Ala92-Dio2 mice were created using CRISPR/Cas9 system on a B6 background. Ala92-Dio2 mice breed and grow normally (Supplemental Figure 1A), exhibiting normal circulating levels of TSH, T4 and T3 (Supplemental Figure 1B) and D2 kinetics with a Km[T4] ~1.9nM (Supplemental Figure 1C). No differences were observed in body weight and food intake (Supplemental Figure 1A and D). Systemic euthyroidism was further documented by absence of hypothyroid-like features in the Ala92-Dio2 skeleton (Supplemental Figure 1E-V).

Discrete brain areas were studied using an unbiased whole-transcript microarray approach (Ala92-Dio2 homozygotes *vs* Thr92-Dio2 homozygotes; Table S2-11). Midline 1 (*Mid1*), which encodes a microtubule associated protein with E3 ubiquitin ligase activity involved in the Opitz syndrome (45), was the only common gene differentially expressed in all five brain areas: 2.4-3.7-fold lower mRNA levels in the Ala92-Dio2 mouse brain ($p<0.001$). Gene set enrichment analysis (GSEA; p<1%; Table S12-21) identified several gene sets related to ERGIC, Golgi or ubiquitin proteasome system in the amygdala (Table S12), cerebellum (Table S14), prefrontal cortex (Table S18) and striatum (Table S20), including the top-2 gene sets in the pre-frontal cortex, which were ERGIC-related (Table S18). The more sensitive RT-qPCR indicated widespread elevation of *Bip* mRNA levels (Table 1). Other UPR-related genes were also activated in cortex, particularly the Atf6 pathway (Table 1) and increased levels of cleaved ATF6 in sonicates of Ala92-Dio2 cortex (Figure 4A-B); s*Xbp1* mRNA levels were also elevated by 40% in the cortex of Ala92-Dio2 mice (Table 1). The amygdala was particularly affected, with 51% elevation in *Bip*, 54% in *Ergic53* and *Pdi*, and 59% elevation in *sXbp1* mRNA levels (Table 1).

Slower rate of T4 to T3 conversion in intact cells expressing Ala92-D2^{HY}

The in vitro kinetics (Km[T4]) of Ala92-D2^{HY} and Thr92-D2^{HY} are indistinguishable in cell sonicates (25). However, here we saw that in intact cells the ability of D2 to convert T4 to T3 is diminished by the Thr92Ala substitution (Figure 4C). Ala92-D2^{HY}-cells incubated with 10pM (physiological) or 50pM free ^{125}I-T4 produced ~30% less T3 over 24h when compared with Thr92-D2^{HY} cells. At the same time, Ala92-D2^{HY} protein levels (Figure 4D) and activity (Figure 4E) in cell sonicates were undistinguishable from Thr92-D2^{HY} sonicates. These contrasting results could reflect limited availability or efficacy of the in vivo cofactor; when assayed in vitro, cells are broken and cofactor is abundant in the form of DTT. To test whether Golgi distribution affects Ala92-D2^{HY} activity, we measured T3 production in intact Ala92-D2^{HY}-cells that had been treated overnight with 4-PBA or cholesterol (as in Figure 3K,X). Treatment with 4-PBA increased T3 production rate in Ala92-D2^{HY}-cells to the level observed in Thr92-D2^{HY}-cells (Figure 4F). The

effect of cholesterol saturation was less clear, as T3 production in cholesterol treated Ala92-D2^{HY}- cells remained below control levels (Figure 4F).

There is localized hypothyroidism in the Ala92-Dio2 brain

To study T3-TR signaling in the different brain areas, two custom-made gene sets containing 33 T3-responsive genes were prepared for GSEA: (i) 19 positively regulated genes (Table S22) and (ii) 14 negatively regulated genes (Table S23). There is evidence of reduced T3-TR signaling in the Ala92-Dio2 striatum (Supplemental Figure 2): positively T3-regulated genes were enriched in the Thr92-Dio2 brain whereas negatively T3-regulated genes were enriched in the Ala92-Dio2 brain. These striatal differences were confirmed by measuring a positively and a negatively T3-regulated gene, i.e. *Ier5* and *Odf4* via RT-qPCR (Table S24). In the Ala92-Dio2 amygdala and prefrontal cortex, only the positively T3-regulated genes were affected (Supplemental Figure 2). In the hippocampus and cerebellum, differences between Thr92-Dio2 and Ala92-Dio2 animals were observed at the FDR q-value (0.15-0.24) but not at the much stricter p-value level (Supplemental Figure 2).

A component of the brain adaptation to hypothyroidism is a regional specific increase in D2 activity via transcriptional and post-transcriptional mechanisms that mitigates the effects of hypothyroidism on brain (46). Indeed, the Ala92-Dio2 mouse exhibits a 1.6-2.0-fold increase in *Dio2* mRNA and D2 activity in prefrontal cortex, hippocampus and cerebellum whereas in the striatum and amygdala - the two areas that exhibit decreased T3-TR signaling - such a response was not observed (Table 2).

Ala92-Dio2 mice are sensitive to an anxiogenic environment

The open field test was performed under low intensity red light to minimize anxiety. Ambulatory activity was not different (Supplemental Figure 3B-C) but exploratory activity was higher in Ala92-Dio2 mice (Supplemental Figure 3D-E). Moving the animals to the elevated plus maze, a typical anxiogenic platform, resulted in Ala92-Dio2 mice exhibiting higher ambulatory/exploratory activities (Supplemental Figure 3G-L) and more risk assessment behavior (Supplemental Figure 3M) when compared to Thr92-Dio2 mice. The pattern of higher mobility in Ala92-Dio2 mice was maintained during the highly anxiogenic tail suspension studies (Supplemental Figure 3N-O).

Once settled, Ala92-Dio2 mice refrains from physical activity and exhibits sleepiness and impaired memory

The hypersensitivity to the environment prompted us to study Ala92-Dio2 mice in their homecage, while they were housed in a comprehensive lab animal monitoring system (CLAMS) and monitored 24/7. Once settled in an environment of low anxiety, Ala92-Dio2 mice travelled ~30% shorter distances, exhibited a ~9% slower nightly VO2 and slept ~4.2-times longer when compared to Thr92-Dio2 mice (Table 3 and 5). This was not due to an impaired motor function given that in separate experiments mice ran on a treadmill for approximately 21 min and reached speeds of ~28 m/min, regardless of genotype. These measurements were repeated while animals had voluntary access to a spinning wheel for 3 days. Ala92-Dio2 mice used the

wheel about half as much as Thr92-Dio2 mice (Table 3 and 6), with a reduced nightly VO2 during the same time period (Table 3 and 6). Despite the exercise stimulus, Ala92-Dio2 mice continued to travel ~15% less and slept 3.6-times longer as compared to Thr92-Dio2 mice (Table 3 and 6).

Cognition was tested through the novel object recognition (NOR) and the valence-based social interaction (SI) tests, which rely on exploratory behavior and assess memory and preference for novelty. In the NOR and SI test, animals of both genotypes explored the objects/subjects similarly during the familiarization period (Supplemental Figure 4 and 5), with Thr92-Dio2 mice passing the 3h-recall by focusing preferentially on the new object (Figure 5A). In contrast, the Ala92-Dio2 mice failed the 3h recall test, dedicating similar amounts of time to old and new objects (Figure 5A). Later, both Ala92-Dio2 and Thr92-Dio2 mice did well on the second recall 24h later (Figure 5B). The SI test uses conspecific animals and thus memory formation is strengthened by emotionally salient experiences. While Thr92-Dio2 mice passed the 3h- and 24h- recalls (Figure 6A-B), Ala92-Dio2 mice barely passed the 3h-recall (statistically borderline; Figure 6A) but did well on the 24h-recall (Figure 6B).

Short-term treatment with LT3 partially rescues the Ala92-Dio2 mouse phenotype

In an attempt to increase T3-TR signaling and rescue the Ala92-Dio2 mouse phenotype, Thr92-Dio2 and Ala92-Dio2 mice were treated with LT3 (1ug/day●10 days); as expected, serum TSH became suppressed (Table 3). LT3 dissipated differences in distance travelled and VO2, but Ala92-Dio2 mice continued to sleep ~2.2-times longer when compared to Thr92-Dio2 mice (Tables 3 and 5). During the 3-day exercise period, Ala92-Dio2 mice travelled around the cage as much as Thr92-Dio2 mice while exhibiting a similar VO2, but still slept ~2.1-times longer (Tables 3 and 5) and used the spinning wheel about half as much as the Thr92-Dio2 mice (Tables 3 and 6). LT3 improved performance of Ala92-Dio2 mice on the NOR (Figure 5C-D) and SI tests (Figure 6C-D), albeit LT3-treated Ala92-Dio2 mice continued to perform worse than Thr92-Dio2 mice in the 3h-recall (Figure 5C); as before, no differences between genotypes were observed at the 24h-recall (Figure 5D). Performance of both groups of LT3-treated animals was indistinguishable during the 3h- and 24h-recalls in the SI test (Figure 6C-D).

Treatment with 4-PBA rescues the Ala92-Dio2 mouse phenotype

In order to evaluate how much of the Ala92-Dio2 mouse phenotype is due to ER stress and UPR activation, intact Thr92-Dio2 and Ala92-Dio2 mice were given 4-PBA (0.25g/Kg BW/day●20 days) to restore proteostasis; 4-PBA normalized UPR markers in different brain areas (Table S25). 4-PBA-treated Ala92-Dio2 animals travelled similar distances to Thr92-Dio2 mice and slept similarly (Table 3 and 5); VO2 is also not different between groups (Table 3 and 5). Similarly, during the 3-day exercise period, Ala92-Dio2 mice travelled in the home-cage as much as Thr92-Dio2 mice (Table 3 and 6). A dramatic effect of 4-PBA treatment was to dissipate of differences in utilization of the spinning wheel and VO2 between Ala92-Dio2 and Thr92-Dio2 mice (Table 3 and 6). Treatment with 4-PBA also normalized performance of Ala92-Dio2 mice on the NOR (Figure 5E-F) and SI tests (Figure 6E-F).

Differences between Thr92-Dio2 and Ala92-Dio2 mice remain during hypothyroidism

After 5-6 weeks on MMI all animals developed overt hypothyroidism, with high serum TSH levels (Table 3). Hypothyroid Ala92-Dio2 mice traveled ~20% less as compared to hypothyroid Thr92-Dio2 mice (Table 3 and 5), and maintained a 7.5-10% slower VO2 (Table 3 and 5). Sleeping duration increased by ~460% in hypothyroid Thr92-Dio2 mice and by ~25% in Ala92-Dio2 mice, eliminating the differences between genotypes (Table 3 and 5). Exercise in the spinning wheels stimulated motor activity in all animals but hypothyroid Ala92-Dio2 mice continued to travel shorter distances in the cage (~50% less) when compared to Thr92-Dio2 mice (Table 3 and 6). Notably, only in hypothyroid Thr92-Dio2 mice did exercise shorten the sleeping duration by half (Table 3 and 6). Likewise, Ala92-Dio2 mice used the spinning wheel about half as much as Thr92-Dio2 mice (Table 3 and 6) and exhibited slightly slower nightly VO2 (Table 3 and 6). Cognition was markedly affected by hypothyroidism, regardless of genotype. All hypothyroid animals failed the 3h- and 24h-recall on the NOR test (Figure 5G-H). Whereas all animals failed the 3h-recall on the SI test, only Thr92-Dio2 mice managed to pass the 24h-recall (Figure 6G-H).

Chronic treatment with LT4 minimally improves memory in hypothyroid Ala92-Dio2 mice; full response with LT4+LT3

All hypothyroid animals were implanted with subcutaneous pellets to deliver stable amounts of LT4 or LT4+LT3 for an additional 6 weeks, which respectively normalized (Thr92-Dio2: 3.5±0.45 vs. Ala92-Dio2: 2.02±0.69; n=5-6) or suppressed serum TSH (Thr92-Dio2: 0.04±0.002 vs. Ala92-Dio2: 0.03±0.001; n=6). Treatment with LT4 eliminated the differences between Thr92-Dio2 and Ala92-Dio2 mice previously observed in home-cage assessment, including movement, sleeping time and VO2 (Table S26). However, LT4 alone failed to fully restore performance in the memory tests. Thr92-Dio2 mice responded to LT4 by passing the NOR and SI 3h-recall tests but failed the 24h-recall on both tests (Figures 5I-J and 6I-J). In contrast, Ala92-Dio2 mice did not respond to LT4 and failed NOR test 3h- and 24h-recalls; only a partial improvement in the SI test 3h-recall was observed in Ala92-Dio2 mice (Figures 5I-J and 6I-J). Notably, treatment with LT4+LT3 normalized memory scores in all animals, regardless of genotype (Figures 5K-L and 6K-L).

Discussion

Previous studies in which added *N*- or *O*-glycosylation sequences failed to direct Golgi-specific D2 glycosylation led to the conclusion that D2 is retained in the ER (17). Here we specifically studied the Golgi apparatus, having found that Thr92-D2^{HY} indeed resides in the ER but also recycles between ER and cis-Golgi via ERGIC, keeping a minimal presence in the cis-Golgi (Figure 1A-F). In contrast, Ala92-D2^{HY} causes ER stress and can be easily visualized in the trans-Golgi (Figure 1G-L). This occurs as a result of protective mechanisms that restore cellular proteostasis, increased expression of ERGIC53 and activation of the SCAP pathway.

A slower enzyme reactivation could explain the ensuing ER stress in Ala92-D2^{HY}-cells. Conformational changes in D2 during catalysis include formation of an intramolecular selenenylsulfide that requires cofactor-mediated resolution before the enzyme is ready for a new round of deiodination (47, 48). That Ala92-D2^{HY}-expressing cells produce less T3 (Figure 4C) suggests that

reactivation of Ala92-D2 is slower given that Ala92-D2 exhibits similar Km[T4] (Supplemental Figure 1C) and, in Ala92-D2^{HY}-cells, D2 protein (Figure 4D) and in vitro activity (Figure 4E) are preserved. Furthermore, an extended life of the oxidized selenenylsulfide linkage also explains the finding of altered redox state in Ala92-D2^{HY}-cells (19). Therefore, Ala92-D2 is likely trapped in an altered molecular configuration (the selenenylsulfide) with slower catalytic activity, which in turn triggers ER stress and activates UPR to restore proteostasis. This is supported by the observation that the enhanced folding capacity in Ala92-D2^{HY}-cells provided by 4-PBA ends ER stress/UPR (Table S1), reduces Ala92-D2^{HY} in the trans-Golgi (Figure 3K-Q), accelerates D2-mediated T3 production (Figure 4E) and dissipates most of the Ala92-Dio2 phenotype in vivo (Table 3-6; Figure 5).

The buildup of Ala92-D2^{HY} in the trans-Golgi likely results from binding to the p97-Ubdx1 protein complex that delivers Ala92-D2^{HY} to ERGIC53 (33). Normally, Thr92-D2^{HY} is retrotranslocated to the cytoplasm via interaction with the p97-Ataxin-3 (Atx3) complex, deubiquitinated and delivered to the proteasomes (32). However, the extended Ala92-D2^{HY} half-life indicates this process is impaired (19). Under ER stress, the 2-3-fold higher levels of ERGIC53 (Figure 2O-Q) enhances the formation of UBXD1-ERGIC-53 complex (33) that binds to Ala92-D2^{HY}-p97 (Figure 1M-N), directing Ala92-D2^{HY} to the Golgi instead of the proteasomes. The critical role played by ERGIC53 in this process is illustrated by findings in *ERGIC53*$^{-/-}$ cells, which exhibit less colocalization of Ala92-D2^{HY} with the cis-Golgi marker GM130 (Figure 3A-H). SCAP (Figure 3I-J) might constitute an additional pathway, which is also activated by ER stress (43, 44). However, the fact that cholesterol saturation reduced only slightly Ala92-D2^{HY} colocalization with the trans-Golgi marker p230 (Figure 3R-X) suggests this is a secondary mechanism.

There is ample evidence that ER stress/UPR (49) and disruption of T3-TR signaling (50) can interfere with neuronal function and lead to impaired cognition. For example, mice with astrocyte-specific inactivation of Dio2 are systemically euthyroid but exhibit anxiety-depressive-like behavior due to generalized hypothyroidism in the brain (51). In addition, a transgenic mouse bearing a mutant *TRβ1* is systemically euthyroid but displays behavioral abnormalities such as inattention, hyperactivity and impulsivity, a phenotype that is dynamic and sensitive to environmental changes (52); this is reminiscent of our findings in the Thr92Ala-Dio2 mouse. That the Ala92-Dio2 brain exhibits hypothyroid areas was confirmed by the observation that short-term treatment with LT3 improved cognition (Table 4 and Figures 5-6) and physical activity (Tables 3 and 5-6) as compared to controls. However, treatment with LT3 caused systemic thyrotoxicosis as evidenced by suppressed serum TSH (Table 3), indicating that the clinical improvement with LT3 administration may carry side effects. The present studies, however, did not allow complete discrimination of how much of the Thr92Ala-Dio2 phenotype is due to localized brain ER stress/UPR, hypothyroidism or both. In fact, in addition to restoring proteostasis 4-PBA also restores Ala92-D2^{HY}-mediated T3 production and could normalize T3-TR signaling in vivo (Figure 4F). The fact that treatment with LT3 markedly improved cognition (Figures 5C-D and 6C-D) whereas 4-PBA restored both motivation (Table 3 and 5) and cognition (Figures 5E-F and 6E-F) indicates that the Thr92Ala-Dio2 phenotype is multifactorial and includes more than one area of the brain, with both ER stress and decreased T3-TR signaling playing an important role.

Despite the obvious phenotype of the Ala92-Dio2 mice, carriers of the Thr92Ala-DIO2 polymorphism are reportedly asymptomatic when surveyed through quality of life- or thyroid-specific-questionnaires (53); a phenotype has only been reported in connection with diagnosis and treatment for hypothyroidism (22, 23). As opposed to the Ala92-Dio2 mice, carriers of the Thr92Ala-DIO2 polymorphism have the opportunity of adjusting through lifelong learning and training, a phenomenon seen in animals (54) and individuals with neurodevelopmental disorders (55). However, it is conceivable that once carriers of the Thr92Ala-DIO2 polymorphism become hypothyroid and are treated with LT4 these adaptive mechanisms are exhausted, bringing out a phenotype that is similar to the Ala92-Dio2 mice. For example, the ~10% lower serum T3 levels observed in adequately LT4-treated hypothyroid patients (7, 9, 56) could be the key element that tips the balance towards behavioral and cognitive dysfunction.

Hypothyroid Thr92-Dio2 mice developed the expected behavior, cognitive and metabolic phenotype that brought them closer to the Ala92-Dio2 phenotype (Tables 3 and 5-6; Figures 5G-H and 6G-H). Notably, their responsiveness to chronic treatment with LT4 was variable. Whereas the metabolic parameters responded similarly to LT4 regardless of the genotype, cognitive parameters were only partially improved (Figures 5I-J and 6I-J). Considering that hypothyroidism therapy is typically lifelong, further improvements with LT4 could have been observed with even longer observation times. Remarkably, treatment with LT4+LT3 normalized all memory scores in all animals (Figures 5K-L and 6K-L) at the expense of suppressing serum TSH.

In depth studies of carriers of the Thr92Ala-DIO2 polymorphism suggest subtle changes in thyroid hormone homeostasis compatible with a slower D2 velocity (57). In addition, depending on race they might be at a higher risk for brain degenerative disease, even as they keep a normal thyroid gland function (20). We found that African Americans (AAs) with Thr92Ala-DIO2 had ~1.3 times higher odds of developing Alzheimer's disease or cognitive impairment not demented, whereas no association was seen in European Americans (EAs); microarray studies confirmed transcriptional patterns of Alzheimer's disease in the temporal pole of AAs carriers of the Thr92Ala-DIO2 polymorphism (20). AAs are known to have a 2-3-fold higher prevalence of cognitive impairment and Alzheimer's disease (58), which could explain their greater susceptibility to the Thr92Ala-DIO2 polymorphism. In addition, the Thr92Ala-DIO2 polymorphism has been associated with increased BMI, insulin resistance (59) and greater risk for type 2 diabetes (18, 60). This suggests that Ala92-DIO2-induced ER stress/localized hypothyroidism could play a broader metabolic role, particularly in tissues that express DIO2 such as human skeletal muscle and brown adipose tissue. Indeed, ER stress is known for reducing insulin receptor signaling, linking obesity, insulin signaling and diabetes (61).

We are hopeful that understanding these mechanisms will accelerate development of new therapeutic approaches for the millions of patients with hypothyroidism and provide justification for clinical studies to assess the utility of customization of thyroid hormone replacement therapy based on their Thr92Ala-DIO2 status. Utilization of 4-PBA in symptomatic hypothyroid patients is an interesting possibility that should be further investigated. In the meantime, given

that some of the Ala92-Dio2 phenotype is reversed by treatment with LT3, albeit it at the expense of serum TSH suppression, it would seem logical to explore further the sensible use of LT3 when treating hypothyroid carriers of the Thr92Ala-DIO2 polymorphism. Of course, the challenge is to deliver T3 in ways that provide stable plasma levels while maintaining serum TSH within normal range and avoiding the risks of systemic thyrotoxicosis.

Materials and Methods

Cell lines and Treatments

HEK-293 cells stably expressing Thr92-D2^{HY} and Ala92-D2^{HY} were described earlier (19). An HEK-293 cell line in which *ERGIC53* gene was inactivated (HEK-*ERGIC53*$^{-/-}$) and the appropriate HEK-293 control cell line were a kind gift from Dr. Jay Yang lab (Univ. of Wisconsin-Madison) (62). Unless specified otherwise, all cells were cultured in high glucose DMEM (Life Technologies) supplemented with 10% fetal bovine serum (Atlanta Biologicals, Flowery Branch, GA) and studied at 70-80% confluency. Whenever cells were incubated with defined amounts of T4 or ^{125}IT4, FBS in the medium was replaced with 0.1% BSA. As indicated, some cells were treated overnight with 100-500uM PBA or 10ug/ml cholesterol. Conversion of T4 to T3 was assessed by incubating cells plated on 6 well dishes (1 million cells/well) with 10pM or 50pM I^{125}-T4 (300,000 cpm/well) and measuring medium ^{125}I^{-} 16 and 40h, which reflects T4 to T3 conversion (63).

FRET Studies

Hydroxypropyl-β-cyclodextrin (HPβCD; Sigma-Aldrich, Budapest, Hungary) and cholesterol (Sigma-Aldrich, Budapest, Hungary) were dissolved in cell media at, respectively, 1.5% and 625μM (64). FRET was performed as described (65), using cells that were plated and transfected (X-tremeGENE HP, Roche, Budapest, Hungary) in 35mm glass-bottom dishes (MatTek Co, Ashland, MA). FRET measurement was performed on the second day after transfection using acceptor-photobleaching on a Nikon A1R laser scanning confocal system in spectral detector mode equipped with Tokai Hit stage top incubator and Supertech temperature controller. The following parameters were applied: 457nm argon-laser for ECFP excitation and 464-500nm range for detection; 514nm argon lasers for EYFP excitation and 516-540nm range for detection. Cells were treated with HPβCD-containing media 2h before imaging. Only cells that exhibited at least 80% bleach efficiency (decrease in EYFP intensity) were analyzed. Calculation of FRET efficiency was based on the increase of the CFP donor signal after photobleaching the YFP acceptor using the following equation: FRET=(ECFP(postbleach)-ECFP(prebleach))/ECFP(postbleach). Data normalization was performed by expressing FRET activity as a percentage of that of the ECFP-EYFP (C-Y) tandem construct (66). ECFP and EYFP (C and Y) monomers were used to determine background. The constructs names reflect the relative position of fluorescent proteins within the fusion (e.g. D2T-EYFP indicates C-terminal YFP fusion to D2 carrying threonine in amino acid position 92). (D2T-EYFP) and D2A- EYFP were previously described (19, 39). SCAP-ECFP was generated by PCR amplification of human SCAP CDS using the following primers, FW 5'- ATTGCTCGAGCCACCATGACCCTGACTGAAAGGC-3' and R 5'- CGGGATCCCGGTCCAGCTTCTCCAGCACAG-3', and fragment was inserted between XhoI-BamHI sites of pECPF-N1 (Clontech, Gote-

borg, Sweden). ECFP-SCAP was generated using the following primers, FW 5'- ATTGCTCGAGC-TATGACCCTGACTGAAAGGC-3' and R 5'- CGGGATCCCGTCAGTCCAGCTTCTCCAGC-3', and fragment was inserted between XhoI-BamHI sites of pECPF-C1 (Clontech, Goteborg, Sweden). WD40 domain-deletion was generated by exchanging the SCAP CDS in the previous constructs to WD40 domain-deleted fragments generated by PCR and using the following primers: SCAPΔWD-ECFP FW 5'- CGGGATCCCGCAGCTCCCCGCGCCTCCGCCG-3' and ECFP-SCAPΔWD FW 5'- CGGGATCCCGGCTCAGCTCCCCGCGCCTCCGCCG-3'. D2T and D2A were generated by PCR amplification of human D2 from D2T-EYFP and D2A-EYFP, respectively, using the following primers; FW 5'-GGAATTCATTATGGGCATCCTCAGCGTAGACTTGCTGATCA-3', R 5'-ATAAGAATGCGGCCGCTTAACCAGCTAATCTAGTTTTCTTACATCTCTTGCT-3', and insertion into pCI-Neo between EcoRI-NotI sites.

Immunofluorescence (IF) Studies

Cells were plated on poly-D-lysine-coated chamber slides; fixation, imaging and co-localization studies were described earlier (67). After fixation in 4% paraformaldehyde (Electron Microscopy Science, Hatfield, PA) for 20min, cells were permeabilized with 0.3% Triton X-100 for 10min, and blocked with Fish Skin Gelatin (Biotum, Fremont, CA) for 1h. Primary antibodies were added at concentration ranging 0.5-5ug/mL at 4°C overnight or 72h when necessary (p230 antibody). Primary antibodies dilution were as follows: 1μg/ml αYFP (Rockland immunochemicals, Pottstown, PA – 600-401-215); α-Golgi antibodies: 0.5μg/ml α-GM130 (Cell Signaling, Danvers, MA – 12480S) or 2μg/ml p230 (BD Biosciences, San Jose, CA - 611280). Secondary antibodies (Life Technologies) were incubated for 1h in the dark; cells were made into a slide using SloFade Gold mounting medium (Life Technologies, Carlsbad, CA). Images were acquired using a Nikon eclipse Ti microscope with C1 confocal system using APO 60x/1.40 oil objective and captured 7 or more z-sections by EZ-C1 software. The images were then analyzed by NISelement AR (Nikon Instruments, Melville, NY) or Image-J software.

Immunoprecipitation Studies

Cells were harvested, suspended in PBS with complete-mini EDTA-free protease inhibitor (Roche, Indianapolis, IN) at 4°C, and lysed with 1% Triton X-100 at 4°C for 30min. After lysis, pH of lysate was adjusted to 7.5. The crosslinker dithiobis-succinimidyl propionate (ThermoFiscer Scientific, Pierce, Waltham, MA) in DMSO was added to final concentration of 5mM and cell lysate incubated on ice for 3h. After crossliking, Tris buffer (pH7.4) was added to the final concentration of 100mM and incubated on ice for 30min for quenching. Cell homogenates were centrifuged for 10min at 800*g* and supernatant fractions collected, which contain cytoplasm and membrane proteins. The supernatant was used for D2 immunoprecipitation. 1μg of rabbit αYFP (Rockland immunochemicals, Pottstown, PA - 600-401-215) or control rabbit IgG (Sigma-Aldrich, St. Louis, MO) were added with 30μl of protein A-agarose and incubated at 4°C overnight. After washing with 1mL of 1% Triton X-100 three times, the beads were treated with SDS-sample buffer for western blot. $D2^{HY}$ immunoprecipitation and western blot were performed as described (32).

Western blot Studies

Western blot analyzes utilized 30µg of total protein or immunoprecipitate pellets. Proteins were resolved on a 4–12% SDS-PAGE gel and transferred to a PVDF membrane (Immobilon-FL, Millipore, Burlington, MA), incubated with indicated antibodies overnight at 4°C and subsequently quantitated with the LiCOR Odyssey instrument with Odyssey Image Studio software using two different infrared channels. The following antibodies were used at indicated dilution: 1:1000, pPERK (Cell Signaling, Danvers, MA – 3179S), 1:500, pEIF2α (ThermoFiscer Scientific, Waltham, MA- MAS-15133),1:500, ATF6 (Santa Cruz Biotechnology, Dallas, TX - 166659), 1:1000, p-IRE1α (Cell Signaling, Danvers, MA – 3294S), 1:1000, ERGIC53 (Sigma-Aldrich, St. Louis, MO - AV46614), 1:1000, p97 (Cell Signaling, Danvers, MA – 2648S), 1:500, Ubxd1 (Abcam, Cambridge, MA - SAB2107374), 1:1000 Bip (Abcam, Cambridge, MA – Ab21685), 1:2500 Dio2 (Abcam, Cambridge, MA – Ab87527) ; when appropriate, 1:1000 dilution of αACTIN (Santa Cruz Biotechnology, Dallas, TX - 166659 – SC-8432) and 1:2500 αCYCLOPHILIN B (Abcam, Cambridge, MA – Ab16045) was used as housekeeping internal control.

Animals

Residue 92 in the murine Dio2 gene is a proline, thus Applied Stemcell, Inc. (Milpitas, CA) was contracted for creation of Thr92-Dio2 and Ala92-Dio2 knockin mice, including generation of guide RNA and utilization the CRISPR/Cas9 system on a C57BL/6 background (68, 69). Two Thr92-Dio2 and three Ala92-Dio2 founders were obtained; the genotype PCR product (~532 bp) of all F1 and F2 mice were sequenced and only those that differed from PP C57BL/6 by the desired SNP at position 92 were bred further; all other animals were euthanized. Founders were mosaic males and were crossed with C57BL/6 wildtype females (Pro92-D2). For genotyping, DNA was extracted with the AccuStart II Mouse Genotyping Kit (Quanta Biosciences, Beverly, MA) and processed through PCR with forward (TGACCATCCTTTATATTGCCTGAC) and reverse (CGGTGCTTCTTAACCTCAAAAGA) primers. PCR product was subjected to EcoNI restriction enzyme digestion. PCR and digestion products were resolved by electrophoresed: the Pro92 DNA is digested by EcoNI (~250bp), whereas Thr92 and Ala92 are not (~532bp); heterozygotes (Thr92/Pro92 or Ala92/Pro92) display two distinct bands; identity of PCR products was confirmed by sequencing. Heterozygote F1s (Thr92/Pro92 and Ala92/Pro92) were crossbred with littermate F1s of identical genotype. Mice were bred and maintained as homozygous Thr92-Dio2 and Ala92-Dio2 colonies. F3 or greater progeny were used for experiments. Unless otherwise specified, male, 8-10-week old animals were used throughout experiments. We are aware that hypothyroidism is more prevalent in females. However, here we focused on males because mood and cognition tests are affected by estrous cycle (70-72). All animals were kept at room temperature (22°C) under a 12-h dark/light cycle, and maintained on a chow diet or low iodine diet, as indicated.

Studies in the Comprehensive Lab Animal Monitoring System (CLAMS)

24h-food intake was measured at the indicated times using the Oxymax feed scale device (Columbus Instruments, Columbus, OH). Oxygen consumption (VO2) and locomotor activity were continuously monitored using the OXYMAX System 5.35, CLAMS (Columbus Instruments, Columbus, OH): X (front to back), Y (right to left), Z (rearing), and distance (ft). Animals were placed in the C.L.A.M.S. with free access to food and water, allowing them to acclimatize in in-

dividual metabolic cages for 48h. Subsequently, metabolic profiles were generated in successive 26-min cycles during 48h with locked wheels and 36h with unlocked wheels (voluntary exercise). Sleep detection were collected using CLAMS-HC program. The application specifies a set of criteria based on animal activity and time that establishes a threshold below which causes the triggering of the onset of a sleep event. Activity is sensed by the traditional IR beam method. Beam interruptions are scored as "counts". The sleep detection parameters used: 4 epoch(s) X 60 s per epoch = 240 s and activity threshold = 0 counts. LT3 was given at 1 ug/day for 10 days. 4-PBA was given at 0.25g/Kg BW/day for 20 days. Hypothyroidism was induced by adding MMI (0.05%) to the drinking water for 6 weeks. Some animals received a subcutaneous implant of LT4 pellet (0.05mg/pellet) or LT4+LT3 (0.025mg/pellet T4 and 0.01mg/pellet T3) that lasted 60 days.

Cognitive and Behavioral Testing

All animals were studied through standard mood and behavior tests, open field (OF)(73), elevated plus maze (EPM)(73), tail suspension (TS)(73). Novel object recognition (NOR) assesses recognition memory by evaluating preference for objects based on their previous encounter with identical two objects or a new object. Results are expressed as a preference index (ratio of the amount of time spent exploring any one of the two objects over the total time spent exploring both objects X 100 (%))(74). Social Interaction (SI) is performed similarly to NOR, except that animals are used instead of objects(75).

Thyroid Function Tests, Tissue Samples and D2 Activity Assay

Animals were euthanized by asphyxiation with CO_2 followed by cervical dislocation. Blood was collected and serum levels of TSH, T4, and T3 measured using a MILLIPLEX rat thyroid hormone panel kit (Millipore, Burlington, MA) and read on a BioPlex (Bio-Rad, Hercules, CA). Whole brain was obtained and dissected for further analyses; pituitary gland and brown adipose tissue were also obtained. Bone samples, as indicated, were harvested from 16-week old male mice and phenotyping studies performed as described (76, 77). D2 activity was assessed in cerebral cortex sonicates from male Thr92-Dio2 and Ala92-Dio2 mice in the presence of 10 mM dithiotreitol, 0.25 M sucrose and 1 nM ^{125}I-(5') T4 (PerkinElmer, Waltham, MA); 1mM propylthiouracil was added to inhibit potential D1 activity and 10 nM T3 to saturate D3 (63).

Microarray Studies

RNA of 5 different brain regions of Thr92-Dio2 and Ala92-Dio2 mice was extracted with the RNeasy Mini Kit (Qiagen, Germantown, MD) and processed for microarray at the Joslin Diabetes Center Genomics Core Laboratory (Boston, MA). Gene expression was determined using Clariom S Mouse array (Affymetrix, Santa Clara, CA). Data were preprocessed using Affymetrix Expression Console. Differential expression analysis was performed with the Affymetrix Transcriptome Analysis Console (TAC) to identify genes with >2-fold or <2-fold change and a nominal P < 5%. Gene ontology analysis was used to determine differences in gene set enrichment (GSEA, Broad Institute, Cambridge, MA) with an FDR <25%, a NES >1.5 and a nominal P <1%. Accession number: GSE119351.

Real-Time Quantitative PCR (RT-qPCR) Studies

Total RNA was extracted from cells lines or brain areas (hippocampus, cerebellum, amygdala, pre-frontal cortex and cerebral cortex) using the RNeasy lipid tissue minikit (Qiagen, Germantown, MD), quantified with a NanoDrop and 0.5–1.0µg used for cDNA synthesis using the Transcriptor first-strand cDNA synthesis kit (Roche, Indianapolis, IN). RT-qPCR conditions were as described (25). Primers were designed to span exon-exon and/or intron-spanning sequences or have been previously validated (https://pga.mgh.harvard.edu/primerbank/); sequences are listed elsewhere (Table S27). Genes of interest were analyzed (Step-One; Applied Biosystems, Foster City, CA) using PerfeCTa SYBR Green Fastmix Rox (Quanta Biosciences, Beverly, MA). The melting curve was used to verify the specificity of the amplicon. Standard curves consisted of 4-5 points of serially diluted mixture of experimental and control group cDNA. Cyclophilin A (*CycloA*), Cyclophilin B (*CycloB*), *18S* rRNA or *βActin* were used as a housekeeping control. The coefficient of correlation was >0.99 for all curves, and the amplification efficiency ranged between 80-110%. Results were expressed as the ratio of test mRNA to housekeeping mRNA.

Statistics

All data were analyzed by PRISM software (GraphPad, La Jolla, CA). Unless otherwise indicated, data are presented as mean ± SEM (Tables) or through box and whiskers plot (Figures); the Mann-Whitney U test was used when the experiment contained two independent groups; if not, the Kruskall-Wallis test was used followed by the Dunn's multiple comparison test. A $p< 0.05$ was used to reject the null hypothesis.

Study Approval

The local Institutional Animal Care and Use Committee at Rush University Medical Center, Chicago, Illinois, US, approved all experiments. IACUC – 16-077 and 15-033.

Acknowledgement

Support from NIDDK DK58538 and DK65055; EU H2020 "Thyrage" No. 666869, the Hungarian Brain Research Program 2.0 - 2017-1.2.1-NKP-2017-00002; The Wellcome Trust Joint Investigator Award 110141/Z/15/Z.

Author contributions

S. J. conducted in vitro experiments with cells, all western blots and prepared figures; data analyzes; T. L. F. and B. M. L. C. B. conducted in vivo experiments, data analyzes, prepared the manuscript figures; G. W. F. microarray analysis and PCRs; D. L. I. Dio2 Km and dissection of bone samples; E. A. M. assisted with the creation of polymorphic animals and dissection of bone samples; A. P. B. brain areas PCRs; R. R. C. exercise tests; P. E. and D. N. FRET experiments; M. M. B. and M. O. R. assisted in the analysis of behavioral phenotype; V. D. L.; N. S. M.; K. F. C. and N. C. B. bone experiments; J. H. D. B. and G. R. W. bone experiments and revision of manuscript; C. F. and B. G. plasmid construction, FRET experiments and manuscript revisions; A. C. B. planned and directed all studies and manuscript write up.

References

1. Chaker L, Bianco AC, Jonklaas J, and Peeters RP. Hypothyroidism. *Lancet.* 2017.
2. Brent GA. Mechanisms of thyroid hormone action. *J Clin Invest.* 2012;122(9):3035-43.
3. Gereben B, Zavacki AM, Ribich S, Kim BW, Huang SA, Simonides WS, et al. Cellular and molecular basis of deiodinase-regulated thyroid hormone signaling. *Endocr Rev.* 2008;29(7):898-938.
4. Jonklaas J, Bianco AC, Bauer AJ, Burman KD, Cappola AR, Celi FS, et al. Guidelines for the treatment of hypothyroidism: prepared by the american thyroid association task force on thyroid hormone replacement. *Thyroid : official journal of the American Thyroid Association.* 2014;24(12):1670-751.
5. Saravanan P, Visser TJ, and Dayan CM. Psychological well-being correlates with free thyroxine but not free 3,5,3'-triiodothyronine levels in patients on thyroid hormone replacement. *J Clin Endocrinol Metab.* 2006;91(9):3389-93.
6. Gereben B, McAninch EA, Ribeiro MO, and Bianco AC. Scope and limitations of iodothyronine deiodinases in hypothyroidism. *Nature reviews Endocrinology.* 2015;11(11):642-52.
7. Gullo D, Latina A, Frasca F, Le Moli R, Pellegriti G, and Vigneri R. Levothyroxine monotherapy cannot guarantee euthyroidism in all athyreotic patients. *PLoS One.* 2011;6(8):e22552.
8. Werneck de Castro JP, Fonseca TL, Ueta CB, McAninch EA, Abdalla S, Wittmann G, et al. Differences in hypothalamic type 2 deiodinase ubiquitination explain localized sensitivity to thyroxine. *The Journal of clinical investigation.* 2015;125(2):769-81.
9. Peterson SJ, McAninch EA, and Bianco AC. Is a Normal TSH Synonymous with "Euthyroidism" in Levothyroxine Monotherapy? *The Journal of clinical endocrinology and metabolism.* 2016:jc20162660.
10. Escobar-Morreale HF, Obregon MJ, Escobar del Rey F, and Morreale de Escobar G. Replacement therapy for hypothyroidism with thyroxine alone does not ensure euthyroidism in all tissues, as studied in thyroidectomized rats. *Journal of Clinical Investigation.* 1995;96(6):2828-38.
11. Samuels MH, Kolobova I, Smeraglio A, Peters D, Purnell JQ, and Schuff KG. Effects of Levothyroxine Replacement or Suppressive Therapy on Energy Expenditure and Body Composition. *Thyroid : official journal of the American Thyroid Association.* 2016;26(3):347-55.
12. Peterson SJ, Cappola AR, Castro MR, Dayan CM, Farwell AP, Hennessey JV, et al. An online survey of hypothyroid patients captured predominantly dissatis-fied individuals. *Thyroid : official journal of the American Thyroid Association.* 2018;28:in press.
13. Crantz FR, Silva JE, and Larsen PR. Analysis of the sources and quantity of 3,5,3'-triiodothyronine specifically bound to nuclear receptors in rat cerebral cortex and cerebellum. *Endocrinology.* 1982;110:367-75.
14. Freitas BC, Gereben B, Castillo M, Kallo I, Zeold A, Egri P, et al. Paracrine signaling by glial cell-derived triiodothyronine activates neuronal gene expression in the rodent brain and human cells. *J Clin Invest.* 2010;120(6):2206-17.
15. Dentice M, Bandyopadhyay A, Gereben B, Callebaut I, Christoffolete MA, Kim BW, et al. The Hedgehog-inducible ubiquitin ligase subunit WSB-1 modulates thyroid hormone activation and PTHrP secretion in the developing growth plate. *Nat Cell Biol.* 2005;7(7):698-705.
16. Zavacki AM, Arrojo e Drigo R, Freitas BC, Chung M, Harney JW, Egri P, et al. The E3 ubiquitin ligase TEB4 mediates degradation of type 2 iodothyronine deiodinase. *Mol Cell Biol.* 2009;29(19):5339-47.
17. Zeold A, Pormuller L, Dentice M, Harney JW, Curcio-Morelli C, Tente SM, et al. Metabolic instability of type 2 deiodinase is transferable to stable proteins independently of subcellular localization. *J Biol Chem.* 2006;281(42):31538-43.

18. Dora JM, Machado WE, Rheinheimer J, Crispim D, and Maia AL. Association of the type 2 deiodinase Thr92Ala polymorphism with type 2 diabetes: case-control study and meta-analysis. *Eur J Endocrinol.* 2010.
19. McAninch EA, Jo S, Preite NZ, Farkas E, Mohacsik P, Fekete C, et al. Prevalent polymorphism in thyroid hormone-activating enzyme leaves a genetic fingerprint that underlies associated clinical syndromes. *J Clin Endocrinol Metab.* 2015;100(3):920-33.
20. McAninch EA, Rajan KB, Evans DA, Jo S, Chaker L, Peeters RP, et al. A Common DIO2 Polymorphism And Alzheimer's Disease Dementia in African And European Americans *The Journal of clinical endocrinology and metabolism.* 2018.
21. McAninch EA, and Bianco AC. New insights into the variable effectiveness of levothyroxine monotherapy for hypothyroidism. *Lancet Diabetes Endocrinol.* 2015;3(10):756-8.
22. Panicker V, Saravanan P, Vaidya B, Evans J, Hattersley AT, Frayling TM, et al. Common variation in the DIO2 gene predicts baseline psychological well-being and response to combination thyroxine plus triiodothyronine therapy in hypothyroid patients. *J Clin Endocrinol Metab.* 2009;94(5):1623-9.
23. Carle A, Faber J, Steffensen R, Laurberg P, and Nygaard B. Hypothyroid Patients Encoding Combined MCT10 and DIO2 Gene Polymorphisms May Prefer L-T3 + L-T4 Combination Treatment - Data Using a Blind, Randomized, Clinical Study. *Eur Thyroid J.* 2017;6(3):143-51.
24. Castagna MG, Dentice M, Cantara S, Ambrosio R, Maino F, Porcelli T, et al. DIO2 Thr92Ala Reduces Deiodinase-2 Activity and Serum-T3 Levels in Thyroid-Deficient Patients. *The Journal of clinical endocrinology and metabolism.* 2017;102(5):1623-30.
25. Canani LH, Capp C, Dora JM, Meyer EL, Wagner MS, Harney JW, et al. The type 2 deiodinase A/G (Thr92Ala) polymorphism is associated with decreased enzyme velocity and increased insulin resistance in patients with type 2 diabetes mellitus. *J Clin Endocrinol Metab.* 2005;90(6):3472-8.
26. Lorente-Rodriguez A, and Barlowe C. Entry and exit mechanisms at the cis-face of the Golgi complex. *Cold Spring Harb Perspect Biol.* 2011;3(7).
27. Appenzeller-Herzog C, and Hauri HP. The ER-Golgi intermediate compartment (ERGIC): in search of its identity and function. *J Cell Sci.* 2006;119(Pt 11):2173-83.
28. Barlowe C, Orci L, Yeung T, Hosobuchi M, Hamamoto S, Salama N, et al. COPII: a membrane coat formed by Sec proteins that drive vesicle budding from the endoplasmic reticulum. *Cell.* 1994;77(6):895-907.
29. Baines AC, and Zhang B. Receptor-mediated protein transport in the early secretory pathway. *Trends Biochem Sci.* 2007;32(8):381-8.
30. Hauri HP, Kappeler F, Andersson H, and Appenzeller C. ERGIC-53 and traffic in the secretory pathway. *J Cell Sci.* 2000;113 (Pt 4):587-96.
31. Meyer H, Bug M, and Bremer S. Emerging functions of the VCP/p97 AAA-ATPase in the ubiquitin system. *Nat Cell Biol.* 2012;14(2):117-23.
32. Arrojo EDR, Egri P, Jo S, Gereben B, and Bianco AC. The type II deiodinase is retrotranslocated to the cytoplasm and proteasomes via p97/Atx3 complex. *Molecular endocrinology.* 2013;27(12):2105-15.
33. Haines DS, Lee JE, Beauparlant SL, Kyle DB, den Besten W, Sweredoski MJ, et al. Protein interaction profiling of the p97 adaptor UBXD1 points to a role for the complex in modulating ERGIC-53 trafficking. *Mol Cell Proteomics.* 2012;11(6):M111 016444.
34. Gaynor EC, te Heesen S, Graham TR, Aebi M, and Emr SD. Signal-mediated retrieval of a membrane protein from the Golgi to the ER in yeast. *The Journal of cell biology.* 1994;127(3):653-65.

35. Schutze MP, Peterson PA, and Jackson MR. An N-terminal double-arginine motif maintains type II membrane proteins in the endoplasmic reticulum. *EMBO J.* 1994;13(7):1696-705.
36. Hsu JW, Tang PH, Wang IH, Liu CL, Chen WH, Tsai PC, et al. Unfolded protein response regulates yeast small GTPase Arl1p activation at late Golgi via phosphorylation of Arf GEF Syt1p. *Proceedings of the National Academy of Sciences of the United States of America.* 2016;113(12):E1683-90.
37. Renna M, Caporaso MG, Bonatti S, Kaufman RJ, and Remondelli P. Regulation of ERGIC-53 gene transcription in response to endoplasmic reticulum stress. *The Journal of biological chemistry.* 2007;282(31):22499-512.
38. Qin SY, Kawasaki N, Hu D, Tozawa H, Matsumoto N, and Yamamoto K. Subcellular localization of ERGIC-53 under endoplasmic reticulum stress condition. *Glycobiology.* 2012;22(12):1709-20.
39. Sagar GD, Gereben B, Callebaut I, Mornon JP, Zeold A, da Silva WS, et al. Ubiquitination-induced conformational change within the deiodinase dimer is a switch regulating enzyme activity. *Mol Cell Biol.* 2007;27(13):4774-83.
40. Mishra AK, Muthamilarasan M, Khan Y, Parida SK, and Prasad M. Genome-wide investigation and expression analyses of WD40 protein family in the model plant foxtail millet (Setaria italica L.). *PloS one.* 2014;9(1):e86852.
41. Espenshade PJ, Li WP, and Yabe D. Sterols block binding of COPII proteins to SCAP, thereby controlling SCAP sorting in ER. *Proceedings of the National Academy of Sciences of the United States of America.* 2002;99(18):11694-9.
42. Brown MS, Radhakrishnan A, and Goldstein JL. Retrospective on Cholesterol Homeostasis: The Central Role of Scap. *Annu Rev Biochem.* 2017.
43. Kammoun HL, Chabanon H, Hainault I, Luquet S, Magnan C, Koike T, et al. GRP78 expression inhibits insulin and ER stress-induced SREBP-1c activation and reduces hepatic steatosis in mice. *The Journal of clinical investigation.* 2009;119(5):1201-15.
44. Werstuck GH, Lentz SR, Dayal S, Hossain GS, Sood SK, Shi YY, et al. Homocysteine-induced endoplasmic reticulum stress causes dysregulation of the cholesterol and triglyceride biosynthetic pathways. *The Journal of clinical investigation.* 2001;107(10):1263-73.
45. Winter J, Basilicata MF, Stemmler MP, and Krauss S. The MID1 protein is a central player during development and in disease. *Front Biosci (Landmark Ed).* 2016;21:664-82.
46. Peeters R, Fekete C, Goncalves C, Legradi G, Tu HM, Harney JW, et al. Regional physiological adaptation of the central nervous system deiodinases to iodine deficiency. *Am J Physiol Endocrinol Metab.* 2001;281(1):E54-61.
47. Schweizer U, Schlicker C, Braun D, Kohrle J, and Steegborn C. Crystal structure of mammalian selenocysteine-dependent iodothyronine deiodinase suggests a peroxiredoxin-like catalytic mechanism. *Proceedings of the National Academy of Sciences of the United States of America.* 2014;111(29):10526-31.
48. Callebaut I, Curcio-Morelli C, Mornon JP, Gereben B, Buettner C, Huang S, et al. The iodothyronine selenodeiodinases are thioredoxin-fold family proteins containing a glycoside hydrolase clan GH-A-like structure. *J Biol Chem.* 2003;278(38):36887-96.
49. Hetz C, and Saxena S. ER stress and the unfolded protein response in neurodegeneration. *Nat Rev Neurol.* 2017;13(8):477-91.
50. Williams GR. Neurodevelopmental and neurophysiological actions of thyroid hormone. *J Neuroendocrinol.* 2008;20(6):784-94.
51. Bocco BM, Werneck-de-Castro JP, Oliveira KC, Fernandes GW, Fonseca TL, Nascimento BP, et al. Type 2 Deiodinase Disruption in Astrocytes Results in Anxiety-Depressive-Like Behavior in Male Mice. *Endocrinology.* 2016;157(9):3682-95.

52. Siesser WB, Zhao J, Miller LR, Cheng SY, and McDonald MP. Transgenic mice expressing a human mutant beta1 thyroid receptor are hyperactive, impulsive, and inattentive. *Genes, brain, and behavior.* 2006;5(3):282-97.
53. Wouters HJ, van Loon HC, van der Klauw MM, Elderson MF, Slagter SN, Kobold AM, et al. No Effect of the Thr92Ala Polymorphism of Deiodinase-2 on Thyroid Hormone Parameters, Health-Related Quality of Life, and Cognitive Functioning in a Large Population-Based Cohort Study. *Thyroid : official journal of the American Thyroid Association.* 2017;27(2):147-55.
54. Lee H, Dvorak D, Kao HY, Duffy AM, Scharfman HE, and Fenton AA. Early cognitive experience prevents adult deficits in a neurodevelopmental schizophrenia model. *Neuron.* 2012;75(4):714-24.
55. Ullman MT, and Pullman MY. A compensatory role for declarative memory in neurodevelopmental disorders. *Neurosci Biobehav Rev.* 2015;51:205-22.
56. Abdalla SM, and Bianco AC. Defending plasma T3 is a biological priority. *Clinical endocrinology.* 2014;81(5):633-41.
57. Butler PW, Smith SM, Linderman JD, Brychta RJ, Alberobello AT, Dubaz OM, et al. The Thr92Ala 5' type 2 deiodinase gene polymorphism is associated with a delayed triiodothyronine secretion in response to the thyrotropin-releasing hormone-stimulation test: a pharmacogenomic study. *Thyroid.* 2011;20(12):1407-12.
58. Potter GG, Plassman BL, Burke JR, Kabeto MU, Langa KM, Llewellyn DJ, et al. Cognitive performance and informant reports in the diagnosis of cognitive impairment and dementia in African Americans and whites. *Alzheimers Dement.* 2009;5(6):445-53.
59. Mentuccia D, Proietti-Pannunzi L, Tanner K, Bacci V, Pollin TI, Poehlman ET, et al. Association between a novel variant of the human type 2 deiodinase gene Thr92Ala and insulin resistance: evidence of interaction with the Trp64Arg variant of the beta-3-adrenergic receptor. *Diabetes.* 2002;51(3):880-3.
60. Nair S, Muller YL, Ortega E, Kobes S, Bogardus C, and Baier LJ. Association analyses of variants in the DIO2 gene with early-onset type 2 diabetes mellitus in Pima Indians. *Thyroid.* 2012;22(1):80-7.
61. Ozcan U, Cao Q, Yilmaz E, Lee AH, Iwakoshi NN, Ozdelen E, et al. Endoplasmic reticulum stress links obesity, insulin action, and type 2 diabetes. *Science.* 2004;306(5695):457-61.
62. Duellman T, Burnett J, Shin A, and Yang J. LMAN1 (ERGIC-53) is a potential carrier protein for matrix metalloproteinase-9 glycoprotein secretion. *Biochem Biophys Res Commun.* 2015;464(3):685-91.
63. Bianco AC, Anderson G, Forrest D, Galton VA, Gereben B, Kim BW, et al. American thyroid association guide to investigating thyroid hormone economy and action in rodent and cell models. *Thyroid.* 2014;24(1):88-168.
64. Christian AE, Byun HS, Zhong N, Wanunu M, Marti T, Furer A, et al. Comparison of the capacity of beta-cyclodextrin derivatives and cyclophanes to shuttle cholesterol between cells and serum lipoproteins. *Journal of lipid research.* 1999;40(8):1475-82.
65. Egri P, and Gereben B. Minimal requirements for ubiquitination-mediated regulation of thyroid hormone activation. *Journal of molecular endocrinology.* 2014;53(2):217-26.
66. Cicchetti G, Biernacki M, Farquharson J, and Allen PG. A ratiometric expressible FRET sensor for phosphoinositides displays a signal change in highly dynamic membrane structures in fibroblasts. *Biochemistry.* 2004;43(7):1939-49.
67. Jo S, Kallo I, Bardoczi Z, Arrojo EDR, Zeold A, Liposits Z, et al. Neuronal hypoxia induces hsp40-mediated nuclear import of type 3 deiodinase as an adaptive mechanism to reduce cellular metabolism. *J Neurosci.* 2012;32(25):8491-500.

68. Aida T, Chiyo K, Usami T, Ishikubo H, Imahashi R, Wada Y, et al. Cloning-free CRISPR/Cas system facilitates functional cassette knock-in in mice. *Genome Biol.* 2015;16:87.
69. Singh P, Schimenti JC, and Bolcun-Filas E. A mouse geneticist's practical guide to CRISPR applications. *Genetics.* 2015;199(1):1-15.
70. McEwen BS, and Alves SE. Estrogen actions in the central nervous system. *Endocr Rev.* 1999;20(3):279-307.
71. Qiu LR, Germann J, Spring S, Alm C, Vousden DA, Palmert MR, et al. Hippocampal volumes differ across the mouse estrous cycle, can change within 24 hours, and associate with cognitive strategies. *Neuroimage.* 2013;83:593-8.
72. Marques AA, Bevilaqua MC, da Fonseca AM, Nardi AE, Thuret S, and Dias GP. Gender Differences in the Neurobiology of Anxiety: Focus on Adult Hippocampal Neurogenesis. *Neural Plast.* 2016;2016:5026713.
73. Hunsberger J, and Duman C. Animal models for depression-like and anxiety-like behavior. *Nature Publishing.* 2007:1-4.
74. Antunes M, and Biala G. The novel object recognition memory: neurobiology, test procedure, and its modifications. *Cogn Process.* 2012;13(2):93-110.
75. Kaidanovich-Beilin O, Lipina T, Vukobradovic I, Roder J, and Woodgett JR. Assessment of social interaction behaviors. *J Vis Exp.* 2011(48).
76. Bassett JH, Gogakos A, White JK, Evans H, Jacques RM, van der Spek AH, et al. Rapid-throughput skeletal phenotyping of 100 knockout mice identifies 9 new genes that determine bone strength. *PLoS Genet.* 2012;8(8):e1002858.
77. Bassett JH, Boyde A, Howell PG, Bassett RH, Galliford TM, Archanco M, et al. Optimal bone strength and mineralization requires the type 2 iodothyronine deiodinase in osteoblasts. *Proc Natl Acad Sci U S A.* 2010;107(16):7604-9.

Tables

Table 1- ER stress-related genes mRNA in brain areas of Thr92-Dio2 and Ala92-Dio2 mice.

Genes	Cortex	Pre-frontal cortex	Hippocampus	Amygdala	Striatum	Cerebellum
Bip	1.37±0.06***	1.13±0.07	1.26±0.08***	1.51±0.19*	1.14±0.05	1.20±0.03**
Chop	1.12±0.05*	1.03±0.06	1.15±0.07	1.20±0.12	1.08±0.04	0.99±0.04
sXbp1	1.40±0.14*	1.33±0.19	1.06±0.06	1.59±0.16**	0.93±0.08	1.16±0.12
Ergic53	1.08±0.08	1.03±0.07	0.97±0.09	1.54±0.18*	1.04±0.07	1.05±0.06
Pdi	1.20±0.07*	0.92±0.03	0.99±0.05	1.54±0.06***	0.97±0.03	0.95±0.04

Results are fold-change in Ala92-Dio2 relative to Thr92-Dio2 animals; *CycloB* mRNA was used as the housekeeping internal control; gene abbreviations are as indicated in the supplemental Table S27; values are the mean ± SEM of 7-10 independent samples; Statistical analysis used was Mann-Whitney U test vs. Thr92-Dio2 animals; *p≤ 0.05; **p≤ 0.01 and ***p≤ 0.001.

Table 2: *Dio2* mRNA levels and D2 activity in brain areas of Thr92-Dio2 and Ala92-Dio2 mice.

Brain Regions	*Dio2* mRNA	D2 activity	
	Ala92-Dio2	Thr92-Dio2	Ala92-Dio2
Cortex	1.20±0.07*	2.55±0.06	4.05±0.65*
Pre-Frontal Cortex	0.99±0.05	1.14±0.20	2.13±0.30*
Hippocampus	1.24±0.07**	1.46±0.04	2.40±0.31**
Amygdala	1.11±0.11	3.44±0.09	3.53±0.14
Striatum	1.26±0.24	1.53±0.18	1.81±0.29
Cerebellum	0.97±0.06	0.14±0.03	0.28±0.06*

Results are for *Dio2* mRNA are fold-change relative to Thr92-Dio2 animals; *CycloB* mRNA was used as the housekeeping internal control; D2 activity is shown as fmols/mg/h; values are the mean ± SEM of 10-11 independent samples for mRNA and 4-6 independent samples for enzyme activity; Statistical analysis used was Mann-Whitney U test vs. Thr92-Dio2 animals; *p≤ 0.05 and **p≤ 0.01.

Table 3: Metabolic parameters in Thr92-Dio2 and Ala92-Dio2 mice.

Parameter	Reference	Intact animals		LT3-treated animals		4-PBA-treated animals		Hypothyroid animals	
		Thr92-Dio2	Ala92-Dio2	Thr92-Dio2	Ala92-Dio2	Thr92-Dio2	Ala92-Dio2	Thr92-Dio2	Ala92-Dio2
TSH	ng/ml	0.42±0.08	0.45±0.05	<0.03	<0.03	0.78±0.10	0.57±0.01	> 40	> 40
Distance	Fold	1.0±0.08	0.70±0.04[b]	1.0±0.06	0.90±0.04	1.0±0.08	0.84±0.13	1.0±0.01	0.80±0.04[a]
Sleep Time - dark	%	5.8±3.2	23.1±4.8[a]	7±2.1	15.9±3.4[a]	8±1.7	10.8±5.4	12.6±7.0	29.1±1.2[a]
Sleep Time - light	%	7.0±4.5	32.0±6.4[a]	11.1±2.4	24.2±3.0[a]	13±2.2	20±5.4	18.5±9.6	39.9±1.4[a]
VO2 - dark	Fold	1.0±0.01	0.91±0.01[b]	1.0±0.05	1.0±0.05	1.0±0.04	0.98±0.06	1.0±0.01	0.93±0.02[b]
VO2 - light	Fold	0.89±0.03	0.85±0.02	1.0±0.02	1.0±0.05	0.93±0.04	0.93±0.06	0.94±0.03	0.85±0.02[a]
Free access to spinning wheels									
Distance	Fold	2.2±0.16	1.6±0.12[b]	2.5±0.31	2.2±0.24	2.68±0.31	2.51±0.21	2.3±0.21	1.2±0.07[b]
Sleep Time - dark	%	2.1±1.2	18±2.3[b]	10.2±2.3	25.1±1.9[b]	4.3±6.2	18.1±5.9	5.9±1.7	24.9±5.5[a]
Sleep Time - light	%	11.7±6.3	32.3±4.4[a]	16±4.3	32.1±4.3[a]	ND	ND	17.8±5.9	24.5±7.6
Revolutions (24h)	Fold	1.0±0.15	0.51±0.12[a]	1.0±0.21	0.53±0.13[b]	1.00±0.33	0.89±0.13	1.0±0.36	0.47±0.25
Revolutions (72h cum.)	Fold	3.3±0.63	1.6±0.34[a]	4.0±0.17	2.2±0.12[b]	3.7±0.17	3.3±3.02	3.3±0.34	1.6±0.05
VO2 – dark	Fold	1.3±0.08	1.1±0.04[a]	1.3±0.04	1.3±0.02[a]	1.35±0.06	1.23±0.05	1.3±0.08	1.1±0.06[b]
VO2 - light	Fold	0.90±0.04	0.86±0.02	1.1±0.01	1.1±0.02	1.07±0.04	1.08±0.06	0.88±0.03	0.83±0.03

Except for sleep time, results are fold change in Ala92-Dio2 relative to Thr92-Dio2 animals for each specific group; for distance travelled 1.0 = 827, 638, 852 or 1419 ft/48h respectively for intact, LT3-treated, 4-PBA-treated or hypothyroid animals; for VO2 1.0 = 111, 90, 86 or 108 L/Kg•24h respectively for intact, LT3-treated, 4-PBA-treated or hypothyroid animals; for revolutions 1.0 = 23570, 4774, 7196 or 19890 respectively for intact, LT3-treated, 4-PBA-treated or hypothyroid animals; Statistical analysis used was Mann-Whitney U test vs. Thr92-Dio2 animals; [a]$p \leq 0.05$ vs. Thr92-Dio2; [b]$p \leq 0.01$ vs. Thr92-Dio2; ND= no data recorded; all experiments were repeated once with similar results; the four experiments are independent and were not performed simultaneously; they are shown in the same table for convenience; the only statistical comparison is between Ala92-Dio2 mice and Thr92-Dio2 mice under each specific condition; entries are the mean±SEM of 4-6 animals.

Table 4: Summary of observed differences in behavioral tests between Ala92-Dio2 and Thr92-Dio2 mice undergoing the indicated treatments.

Animal	Treatment	NOR		SI	
		3h recall	24h recall	3h re-call	24h recall
Intact	No	↓	↔	↓	↔
Intact	LT3	↔	↔	↔	↔
Intact	4-PBA	↔	↔	↔	↔
Hypothyroid	No	↔	↔	↔	↓
Hypothyroid	LT4	↓	↔	↔	↔
Hypothyroid	LT4+LT3	↔	↔	↔	↔

Data points and statistical analyses are provide in Figures 5 and 6; ↔: no difference with Thr92-Dio2; ↓ impair cognition/memory vs. Thr92-Dio2; NOR: novel object recognition; SI: social Interaction.

Table 5: Summary of observed differences in metabolic parameters between Ala92-Dio2 and Thr92-Dio2 mice undergoing the indicated treatments.

Animal	Treatment		Sleep Time		VO2	
		Distance	**Light**	**Dark**	**Light**	**Dark**
Intact	No	↓	↑	↑	↔	↓
Intact	LT3	↔	↑	↑	↔	↔
Intact	4-PBA	↔	↔	↔	↔	↔
Hypothyroid	Hypothyroid	↓	↑	↑	↓	↓

Data points and statistical analyses are provide in table 3; ↔: no difference with Thr92-Dio2; ↓ diminished distance/VO2 vs. Thr92-Dio2; ↑ increased sleep time vs Thr92-Dio2.

Table 6: Summary of observed differences in metabolic parameters with free access to spinning wheels between Ala92-Dio2 and Thr92-Dio2 mice undergoing the indicated treatments.

Animal	Treatment		Sleep Time		VO2		Revolution	
		Distance	Light	Dark	Light	Dark	24h	72h
Intact	No	↓	↑	↑	↔	↓	↓	↓
Intact	LT3	↔	↑	↑	↔	↓	↓	↓
Intact	4-PBA	↔	ND	↔	↔	↔	↔	↔
Hypothyroid	Hypothyroid	↓	↔	↑	↔	↓	↔	↔

Data points and statistical analyses are provide in table 3; ↔: no difference with Thr92-Dio2; ↓ diminished distance/VO2/revolutions vs. Thr92-Dio2; ↑ increased sleep time vs Thr92-Dio2. ND: no data recorded.

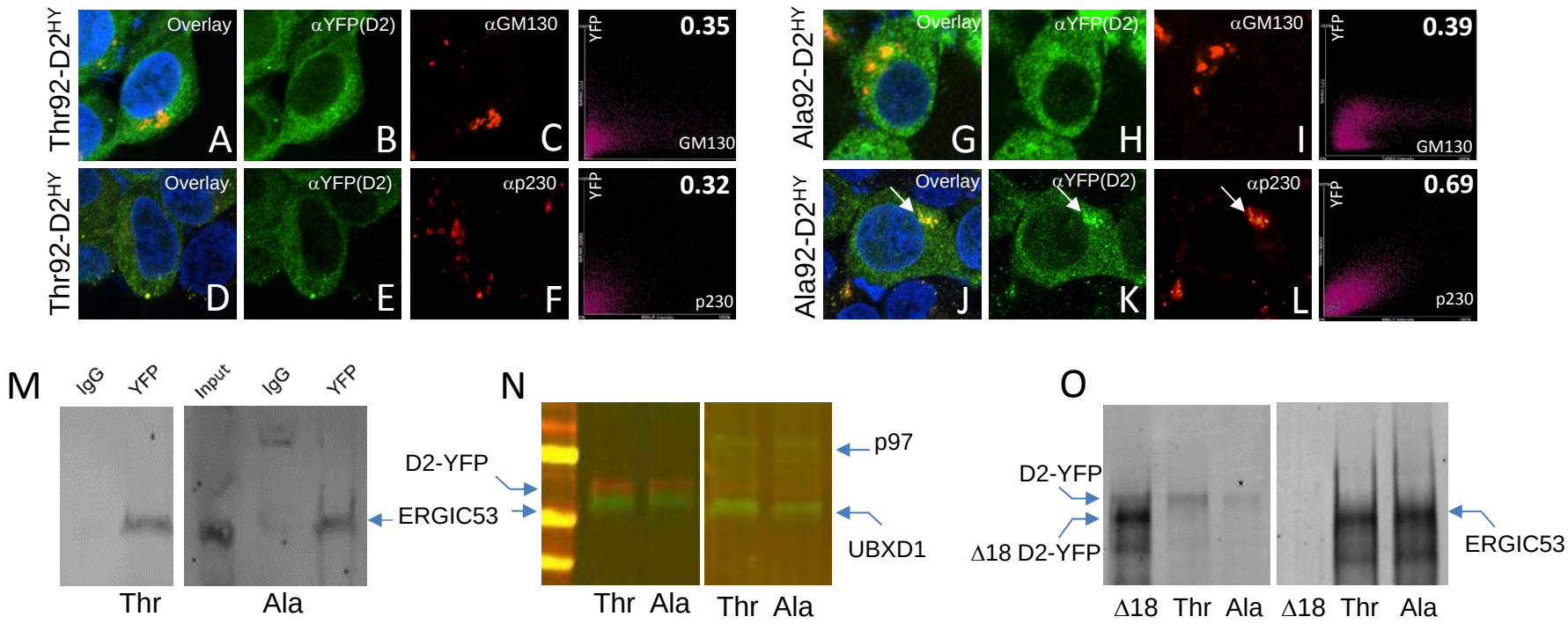
Thr92-D2HY
Overlay
αYFP(D2)
αGM130
YFP
0.35
GM130
A
B
C
Thr92-D2HY
Overlay
αYFP(D2)
αp230
YFP
0.32
p230
D
E
F
Ala92-D2HY
Overlay
αYFP(D2)
αGM130
YFP
0.39
GM130
G
H
I
Ala92-D2HY
Overlay
αYFP(D2)
αp230
YFP
0.69
p230
J
K
L
M
IgG
YFP
Input
IgG
YFP
Thr
Ala
N
D2-YFP
ERGIC53
p97
UBXD1
Thr
Ala
Thr
Ala
O
D2-YFP
Δ18 D2-YFP
ERGIC53
Δ18
Thr
Ala
Δ18
Thr
Ala

Figure 1

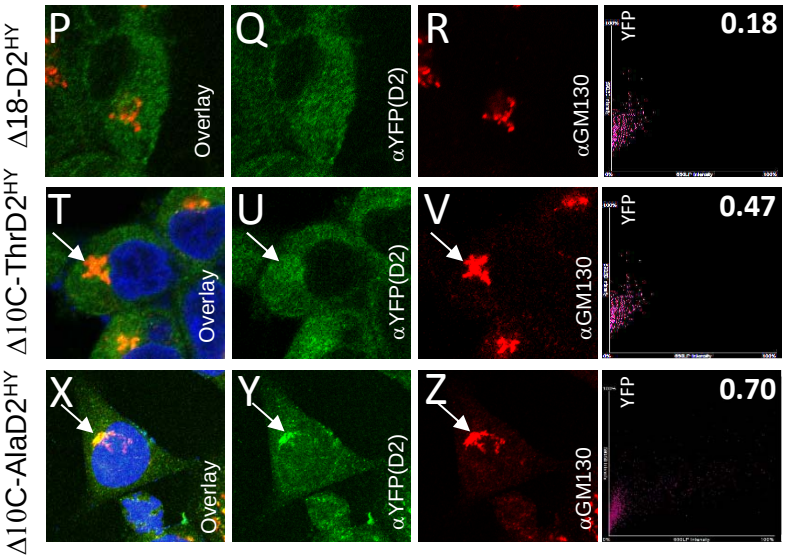

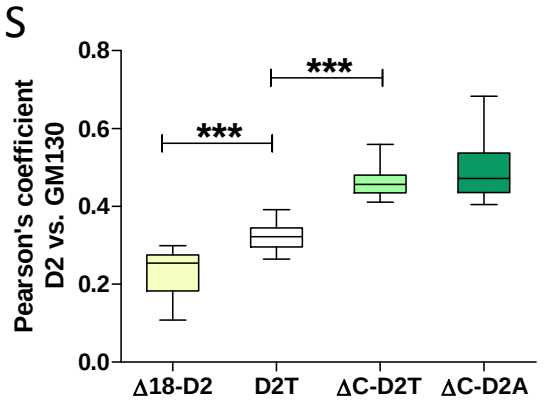

Figure 1: D2 recycles between Golgi apparatus and ER. (A-F) IF of Thr92-D2^{HY}-stably expressing cells using the indicated antibodies; on the far right is the Pearson's plot for each IF; the right top number is the Pearson's coefficient for that specific cell; Person's coefficient: Thr92-DIO2 *x* a-GM130 (0.32±0.06); Ala92-DIO2 *x* a-GM130 (0.36±0.07); **(G-L)** same as (A-F) except that cells stably express Ala92-D2^{HY}; arrow points to Golgi AlaD2 staining; Person's coefficient: Thr92-DIO2 *x* a-p230 (0.33±0.05); Ala92-DIO2 *x* a-p230 (0.65±0.12; p<0.01 *vs* Thr92-DIO2 *x* a-p230); **(M-N)** Thr92-D2^{HY} (Thr) or Ala92-D2^{HY} (Ala) pull down followed by western blot analysis with the indicated antibodies; **(O)** same as (M-N) except that cells transiently express Δ18-D2^{HY}; **(P-R)** same as (A-C) except that cells transiently express Δ18-D2^{HY}; **(S)** Pearson's coefficient between the indicated D2 proteins and cis-Golgi marker GM130; Δ18-D2 is Δ18-D2^{HY} (P-R); D2T is Thr92-D2^{HY} (A-C); ΔC-D2T is Δ10C-Thr92-D2^{HY} (T-V); ΔC-D2A is Δ10C-Ala92-D2^{HY} (X-Z) **(T-Z)** same as (A-C) except that cells transiently express Δ10C-Thr92-D2^{HY} or Δ10C-Ala92-D2^{HY}; magnification: APO 60x/1.40 oil objective; values shown in a box and whiskers plot indicating median and quartiles; n=21/group; Statistical analysis used was Mann-Whitney U test in comparison with D2T; ***p≤0.0001.

Figure 1

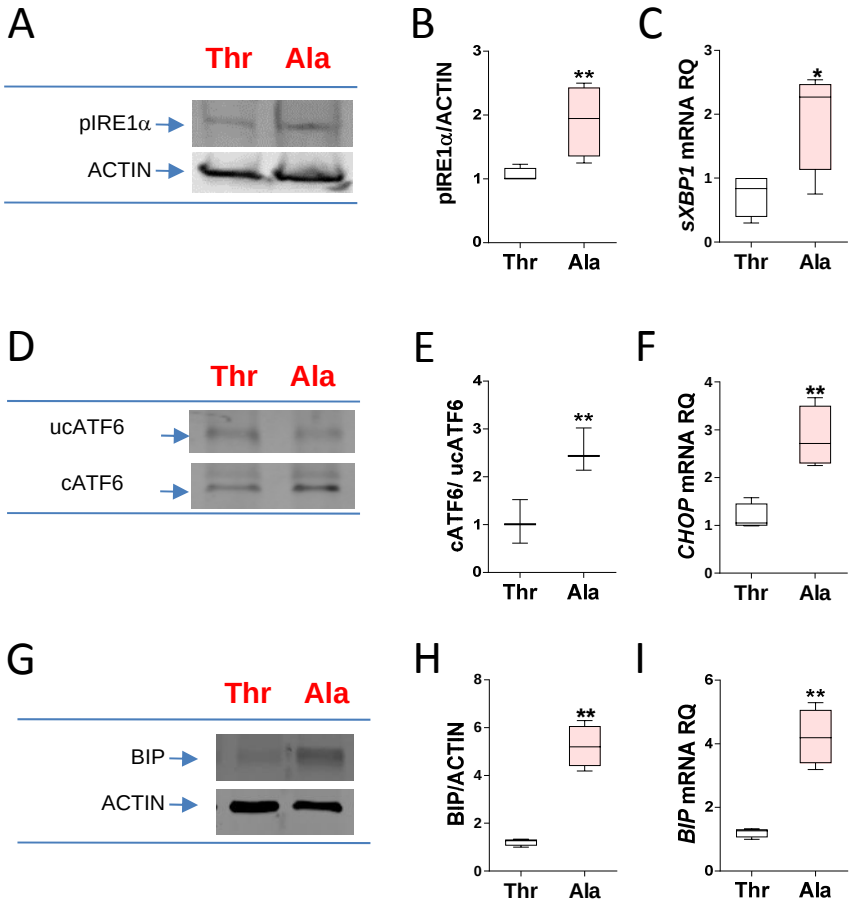
A
Thr
Ala
pIRE1α
ACTIN
B
pIRE1α/ACTIN
**
Thr
Ala
C
sXBP1 mRNA RQ
*
Thr
Ala
D
Thr
Ala
ucATF6
cATF6
E
cATF6/ ucATF6
**
Thr
Ala
F
CHOP mRNA RQ
**
Thr
Ala
G
Thr
Ala
BIP
ACTIN
H
BIP/ACTIN
**
Thr
Ala
I
BIP mRNA RQ
**
Thr
Ala

Figure 2

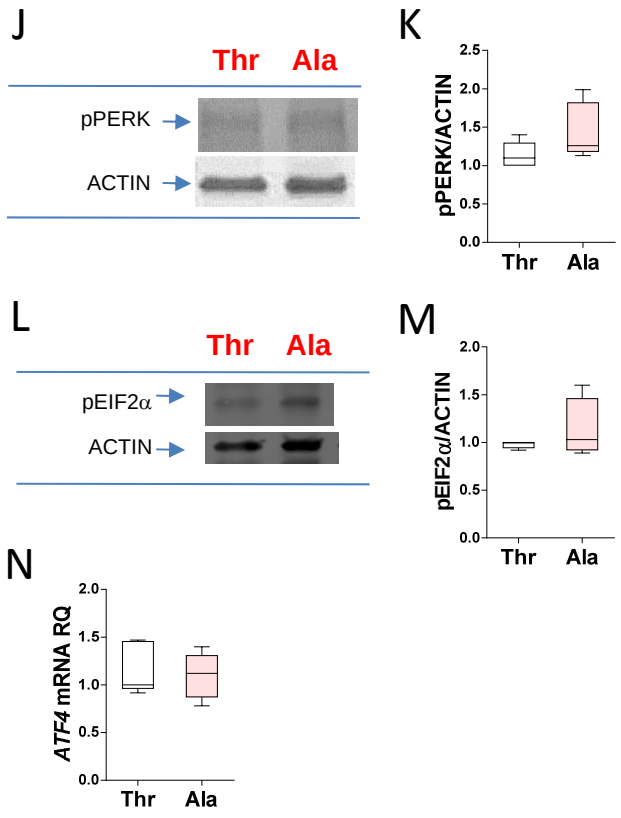
J
Thr
Ala
pPERK
ACTIN
K
pPERK/ACTIN
2.5
2.0
1.5
1.0
0.5
0.0
Thr
Ala
L
Thr
Ala
pEIF2α
ACTIN
M
pEIF2α/ACTIN
2.0
1.5
1.0
0.5
0.0
Thr
Ala
N
ATF4 mRNA RQ
2.0
1.5
1.0
0.5
0.0
Thr
Ala

Figure 2

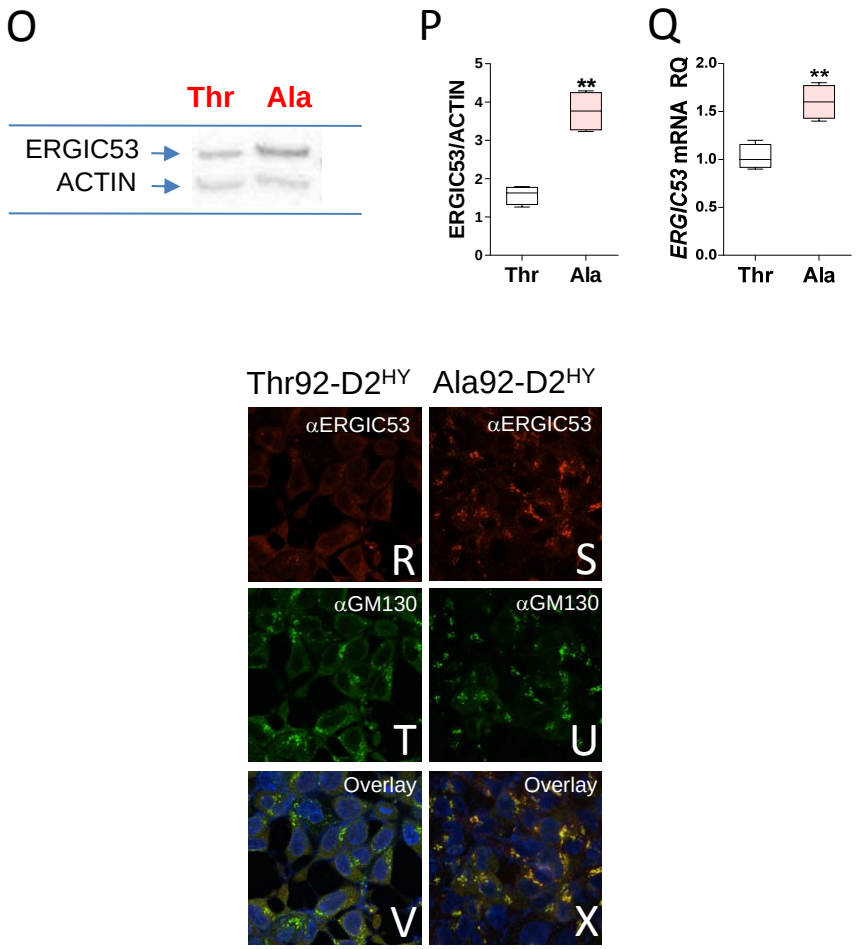

Figure 2: Expression of Ala92-D2 causes ER stress, triggers UPR response. UPR markers in Thr92-D2^{HY} (Thr)- or Ala92-D2^{HY} (Ala)-expressing cells: **(A)** western blot of pIRE1a; **(B)** quantification of pIRE1a shown in (A); **(C)** s*XBP1* mRNA levels; **(D)** western blot of uncleaved (uc) and cleaved (c) ATF6; **(E)** quantification of cATF6 shown in (D); **(F)** *CHOP* mRNA levels; **(G)** western blot of BIP; **(H)** quantification of BIP shown in (G); **(I)** *BIP* mRNA levels; **(J)** western blot of pPERK; **(K)** quantification of pPERK shown in (J); **(L)** western blot of pEIF2a; **(M)** quantification of pEIF2a shown in (L); **(N)** *ATF4* mRNA levels; **(O)** western blot of ERGIC53; **(P)** quantification of ERGIC53 shown in (O); **(Q)** *ERGIC53* mRNA levels; **(R-X)** IF of Thr92-D2^{HY} or Ala92-D2^{HY}-stably expressing cells using the indicating antibodies; magnification: APO 60x/1.40 oil objective; values are shown in a box and whiskers plot indicating median and quartiles; n=4-5/group; Statistical analysis used was the Mann-Whitney U test or the Kruskall-Wallis test was used followed by the Dunn's multiple comparison test; * p≤0.05 and ** p≤0.01.

Figure 2

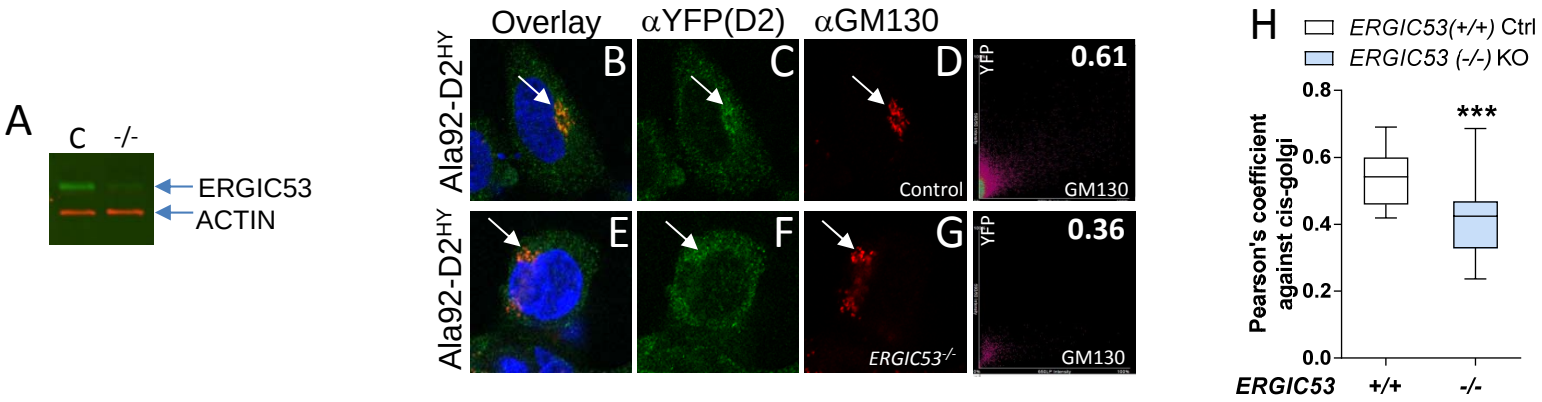
A
C
-/-
ERGIC53
ACTIN
Overlay
αYFP(D2)
αGM130
Ala92-D2HY
Ala92-D2HY
B
C
D
E
F
G
YFP
0.61
Control
GM130
YFP
0.36
ERGIC53-/-
GM130
H
ERGIC53(+/+) Ctrl
ERGIC53 (-/-) KO
Pearson's coefficient against cis-golgi
0.8
0.6
0.4
0.2
0.0
***
ERGIC53
+/+
-/-

Figure 3

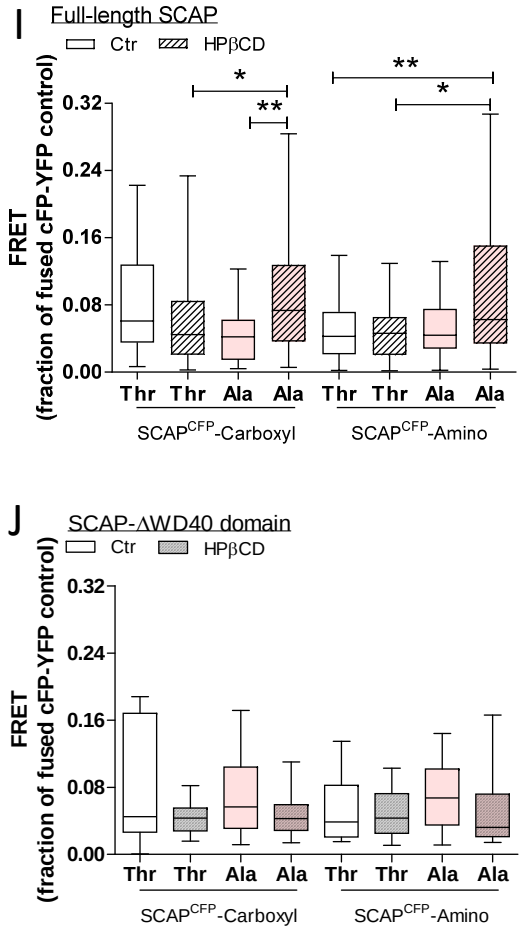
I
Full-length SCAP
Ctr
HPβCD
FRET
(fraction of fused cFP-YFP control)
0.32
0.24
0.16
0.08
0.00
*
**
**
*
Thr Thr Ala Ala Thr Thr Ala Ala
SCAPCFP-Carboxyl
SCAPCFP-Amino
J
SCAP-ΔWD40 domain
Ctr
HPβCD
FRET
(fraction of fused cFP-YFP control)
0.32
0.24
0.16
0.08
0.00
Thr Thr Ala Ala Thr Thr Ala Ala
SCAPCFP-Carboxyl
SCAPCFP-Amino

Figure 3

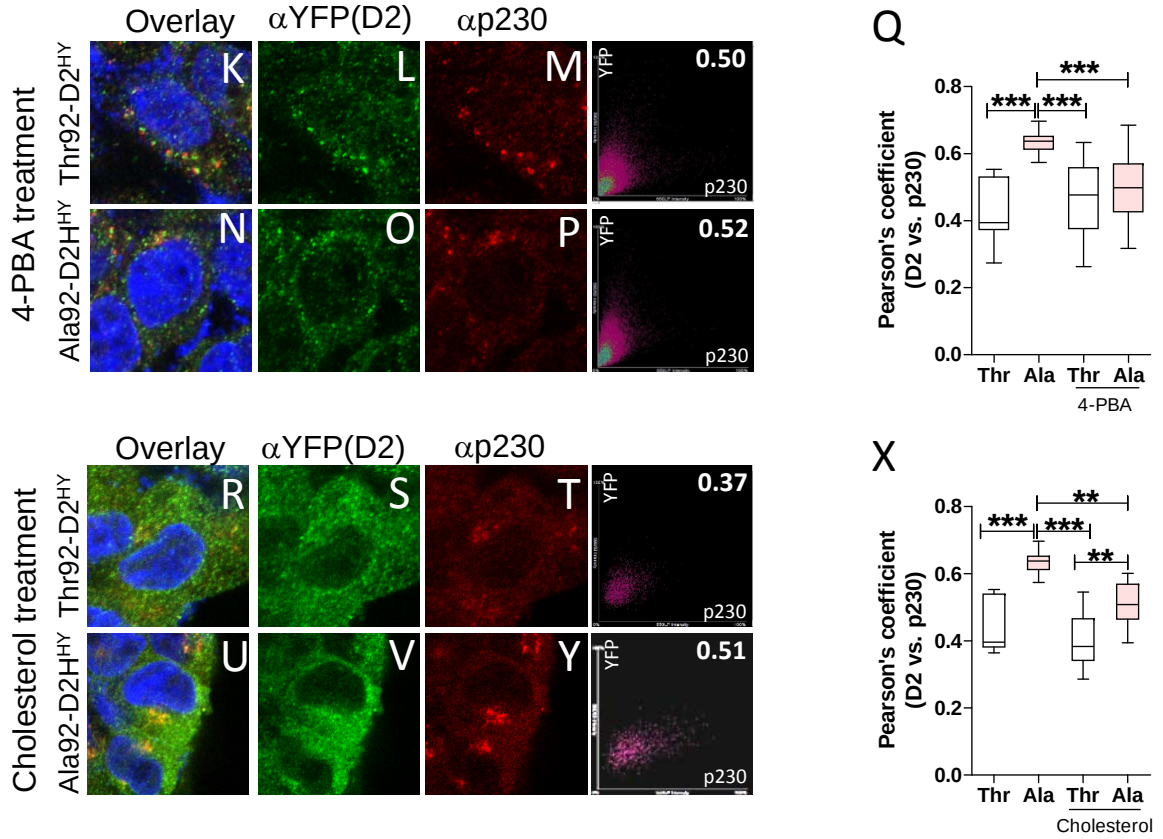

Figure 3: ERGIC53 and SCAP play a role in Ala92-D2 trafficking. (A) western blot of control HEK-293 and HEK-293-*ERGIC*$^{-/-}$ cells using the indicated antibodies; **(B-D)** IF of control HEK-293 cells transiently expressing Ala92-D2^{HY} using the indicated antibodies; on the far right is the Pearson's plot for each IF; the right top number is the Pearson's coefficient for that specific cell; **(E-G)** IF of HEK-293-*ERGIC*$^{-/-}$ cells transiently expressing Ala92-D2^{HY}; arrows point to Golgi AlaD2 staining; **(H)** Pearson's coefficient between the indicated D2 proteins and cis-Golgi marker GM130; **(I)** FRET in HEK293 cells transiently expressing either D2T-EYFP (Thr) or D2A- EYFP (Ala) and SCAP constructs containing the YFP and CFP fluorophores at the indicated positions; cells were treated with HPβCD to cause cholesterol deprivation, as indicated; **(J)** same as (I) except that SCAP-ΔWD40 was used; **(K-P)** IF of Thr92-D2^{HY}- or Ala92-D2^{HY}-expressing cells were incubated overnight with 500uM 4-PBA; **(Q)** Pearson's coefficient between the indicated D2 proteins and trans-Golgi marker p230 as shown in (K-P); **(R-Y)** same as in (K-P) except the cells were incubated overnight with 10ug/ml cholesterol; **(X)** same as in (Q) except that data are from (R-Y); magnification: APO 60x/1.40 oil objective; values are shown in a box and whiskers plot indicating median and quartiles; n=9-69/group; Statistical analysis used was the Mann-Whitney U test or the Kruskall-Wallis test was used followed by the Dunn's multiple comparison test; * p≤0.05, ** p≤0.01 and ***p≤0.001.

Figure 3

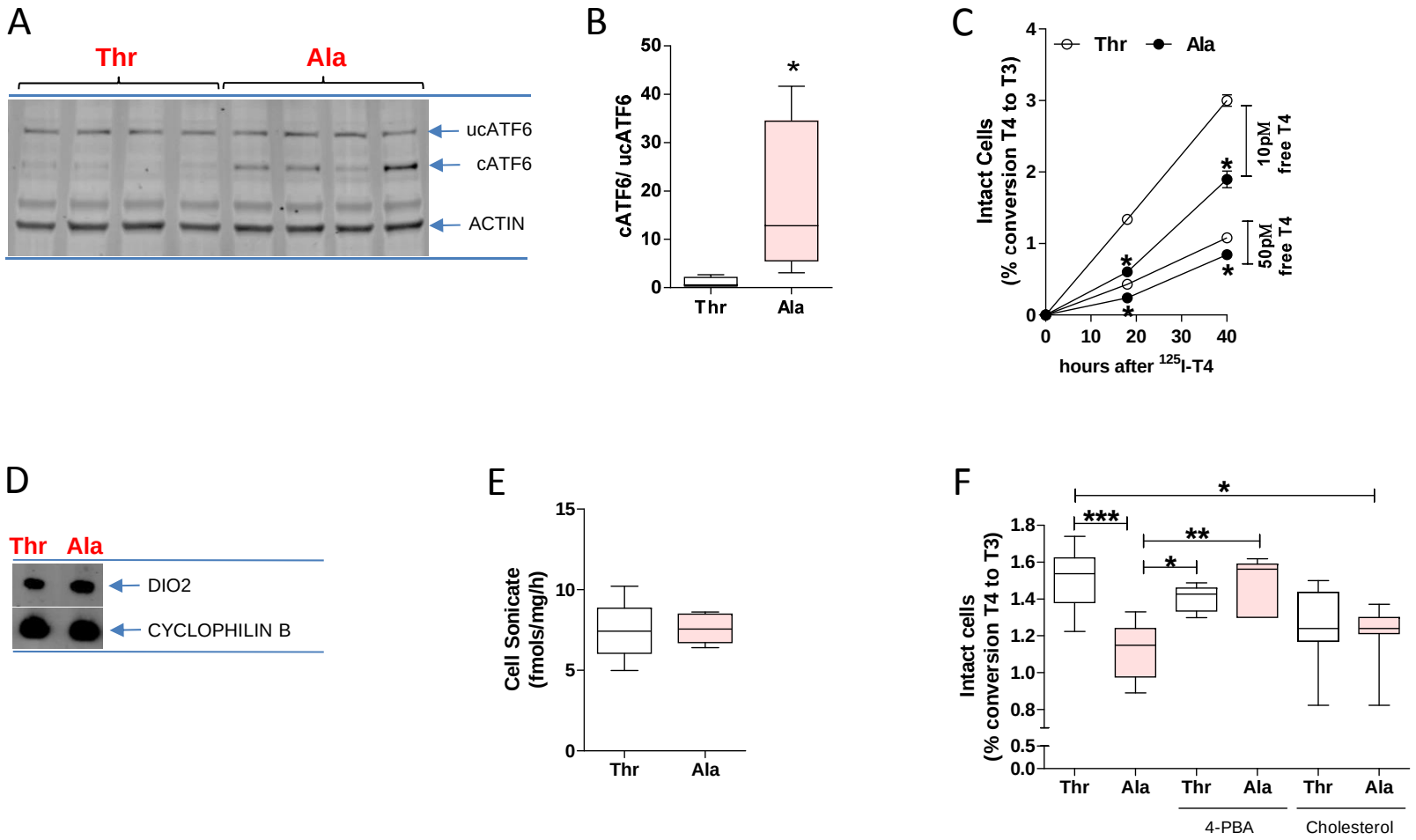

Figure 4: ER stress in Ala92-Dio2 cerebral cortex and slower rate of T4 to T3 conversion in Ala92-D2 expressing cells. (A) western blot of cerebral cortex sonicates of Thr92-Dio2 (Thr) and Ala92-Dio2 (Ala) mice utilizing the indicated antibodies; each lane represents an independent mouse sample; **(B) (B)**quantification of uncleaved (uc) and cleaved (c) ATF6; **(C)** in vivo deiodination in intact Thr92-D2^{HY} (Thr)- or Ala92-D2^{HY} (Ala)-expressing cells; **(D)** immunoprecipitation followed by western blot of T and A cells utilizing α-YFP and α-Cyclophilin B; **(E)** in vitro deiodination in T and A cell sonicates; **(F)** same as in (C), except that cells were treated for 24h with 500uM 4-PBA or 10ug/ml cholesterol; values are shown in a box and whiskers plot indicating median and quartiles or mean±SEM; n=3-10/group; Statistical analysis used was the Mann-Whitney U test or the Kruskall-Wallis test was used followed by the Dunn's multiple comparison test; * p≤0.05, ** p≤0.01 and ***p≤0.001.

Figure 4

Novel Object Recognition

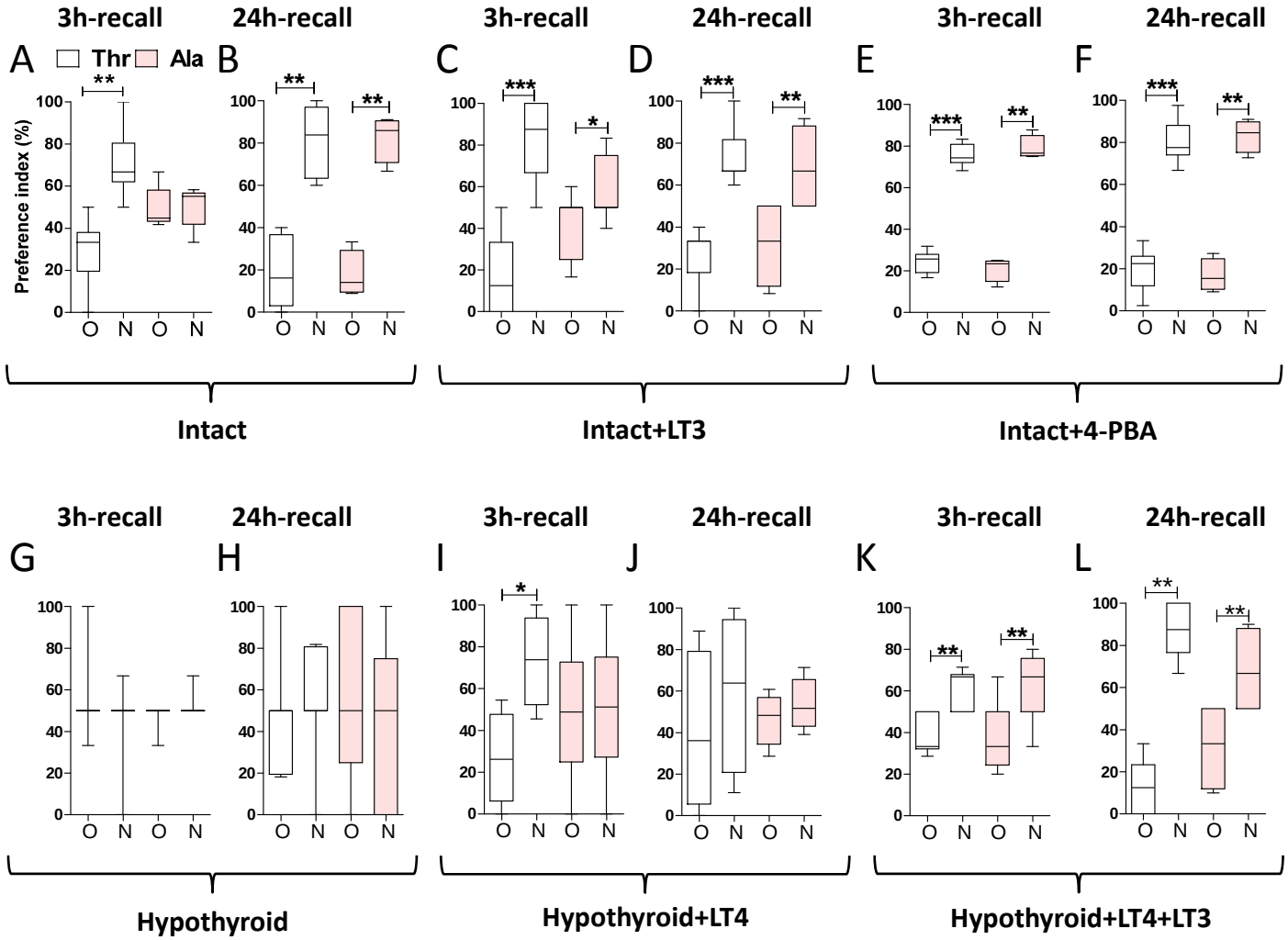

Figure 5: Impaired new object recognition in Ala92-Dio2 mouse. NOR memory test displayed as preference index (%) of Thr92-Dio2 (Thr) and Ala92-Dio2 (Ala) mice. **(A-B)** intact animals; **(C-D)** intact + LT3 animals; **(E-F)** Intact + 4-PBA animals; **(G-H)** hypothyroid animals; **(I-J)** hypothyroid+LT4 animals; **(K-L)** hypothyroid+LT4+LT3 animals; in each plot, N is the new object and O is the old object; **(A,C,E,G,I,K)** 3h-recall; **(B,D,F,H,J,L)** 24h-recall; values are shown in a box and whiskers plot indicating median and quartiles; Statistical analysis used was Mann-Whitney U test; n=5-11/group; * p≤0.05, ** p≤0.01 and ***p≤0.001.

Figure 5

Social Interaction

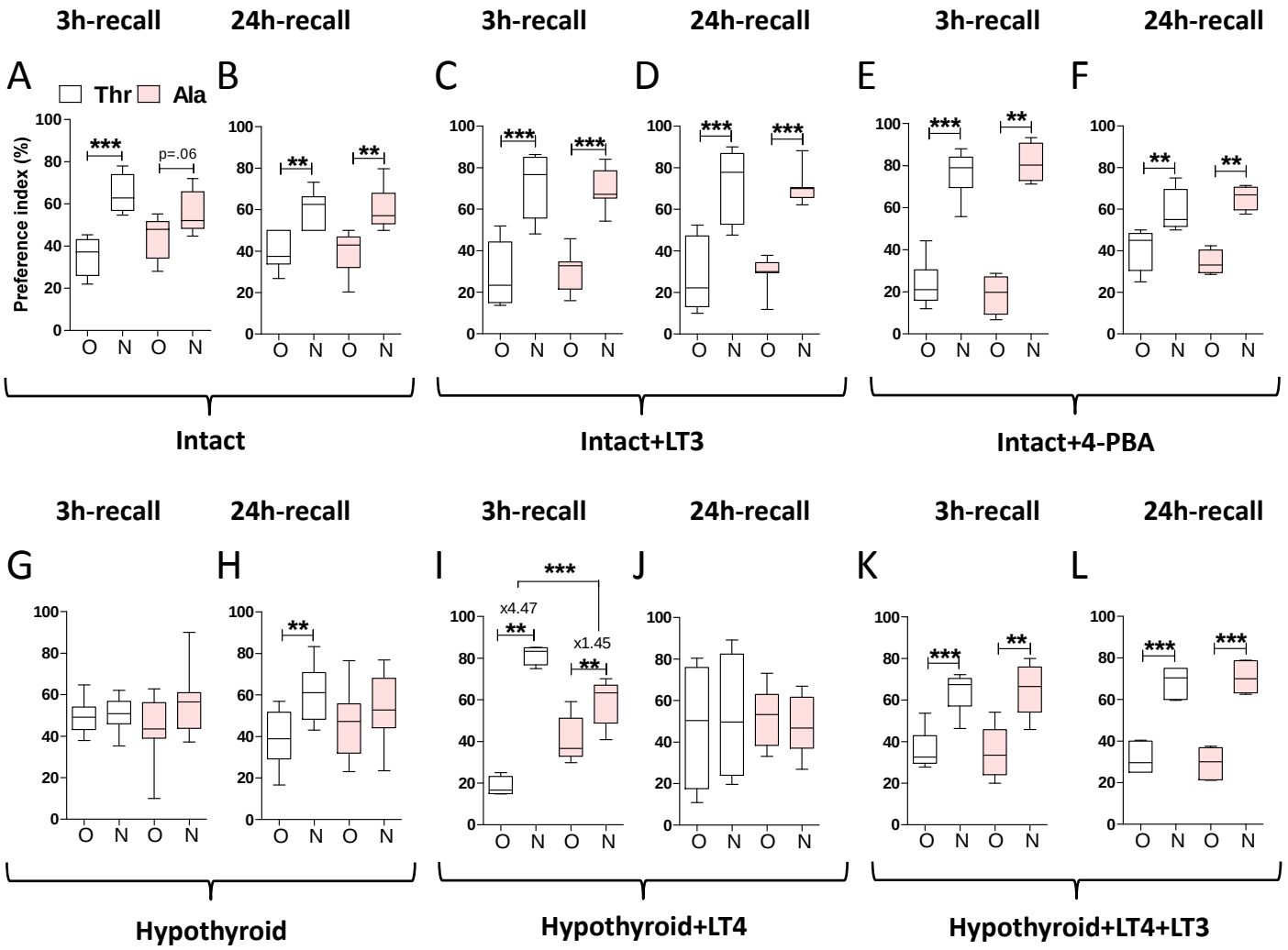

Figure 6: Impaired new social recognition Ala92-Dio2 mouse. SI memory test displayed as preference index (%) of Thr92-Dio2 (Thr) and Ala92-Dio2 (Ala) mice; **(A-B)** intact animals; **(C-D)** intact + LT3 animals; **(E-F)** Intact + 4-PBA animals; **(G-H)** hypothyroid animals; **(I-J)** hypothyroid+LT4 animals; **(K-L)** hypothyroid+LT4+LT3 animals; in each plot, N is the new subject and O is the old subject; **(A,C,E,G,I,K)** 3h-recall; **(B,D,F,H,J,L)** 24h-recall; values are shown in a box and whiskers plot indicating median and quartiles; Statistical analysis used was Mann-Whitney U test; n=5-11/group; * p≤0.05, ** p≤0.01 and ***p≤0.001.

Figure 6